Highly Sensitive Reflective-Mode Phase-Variation Permittivity Sensors Using Coupled Line Sections

Pau Casacuberta, *Graduate Student Member, IEEE,* Paris Vélez, *Senior Member, IEEE,* Jonathan Muñoz-Enano, *Member, IEEE,* Lijuan Su, *Member, IEEE,* and Ferran Martín, *Fellow, IEEE*

***Abstract*—Highly sensitive permittivity sensors operating in reflection and exploiting phase variation are presented in this paper. The sensors are one-port structures implemented by means of a pair of coupled lines, the sensitive region, with an appropriate termination. In particular, it is demonstrated that by either short-circuiting the crossed port to the input port of the device (opening the remaining two ports), or opening the crossed port to the input port (terminating the other two ports with a short-circuit), the sensitivity can be driven to very high values, controlled by the coupling factor. For that purpose, the electrical length of the pair of coupled lines must be set to 90° when such lines are loaded with the reference (REF) material. Thus, the sensitivity is optimized for dielectric constants (the input variable) in the vicinity of the dielectric constant of the REF material, where the indicated phase condition is fulfilled. The output variable is the phase of the reflection coefficient, an easily measurable quantity. For validation purposes, three prototype sensors are designed and fabricated. The achieved sensitivities in two of the fabricated sensors are as high as 659.6° and 736.0°, with figures of merit, or ratio between the maximum sensitivity and the area of the sensing region expressed in terms of the squared-wavelength, of FoM = 9401°/λ^2 and FoM = 12690°/λ, respectively, i.e., very competitive values. Moreover, the indicated high sensitivities and FoMs have been achieved without the need to add further circuit stages to the sensing region, contrarily to other highly-sensitive phase-variation sensors, where sensitivity optimization is achieved at the expense of an increase in the overall sensor size.**

***Index Terms*—Coupled lines, dielectric characterization, microstrip, microwave sensor, phase-variation sensor, reflective-mode sensor.**

I. Introduction

A SIGNIFICANT effort has been recently dedicated to performance improvement and size reduction in the so-called phase-variation microwave sensors [1]–[16]. Although various prototypes of this type of sensors devoted to the measurement of spatial variables have been reported [14]–[16], the most genuine application of phase-variation sensors is dielectric characterization of materials [1]–[13]. Thus, these sensors have been applied to the measurement of the permittivity in material samples, designated as material under test (MUT), and other variables related to it (e.g., concentration of solute content in liquid solutions, material composition, defect detection in samples, etc.).

The canonical output variable in phase-variation sensors is the phase of either the reflection or the transmission coefficient, depending on whether the device operates in reflective- [6]–[8], [12]–[16] or transmission-mode [1]–[5], [9]–[11]. Nevertheless, there are examples of sensors that exploit the variation in the electrical length of the so-called sensing line (caused by the effects of the MUT) where the output variable is not the phase, but the magnitude of a certain transmission coefficient [1], [4], [5]. For that purpose, differential-mode configurations have been proposed, in some cases using artificial sensing lines [1], [4].

An interesting feature of phase-variation sensors is the fact that such sensors can be designed in order to operate at a single frequency, contrary to frequency-variation sensors [17]–[25] and frequency-splitting sensors [26]–[32], which require wideband interrogation signals for sensing (and, consequently, require an associated electronics with higher cost and complexity). Single-frequency sensors based on the modulation of the coupling between a resonant sensing element and a transmission line have also been reported [33]–[43], but such sensors are mostly devoted to the measurement of displacements and velocities. Moreover, coupling-modulation sensors, where the typical output variable is either a voltage or a transmission coefficient magnitude, are less tolerant, as compared to phase-variation sensors, to the effects of electromagnetic interference (EMI) and noise. These advantageous aspects (i.e., single-frequency operation and robustness against EMI and noise) justify the interest for the research in phase-variation sensors.

Reflective-mode phase-variation sensors implemented in planar form [6]–[8], [12], [13], [16] combine the aforementioned advantages of phase measurements with the inherent benefits of operation in reflection, including a simple sensor structure (i.e., a one-port device), and the low profile and cost of planar technology. In addition, reflective-mode sensors can be useful as sensing probes in submersible sensors devoted to the dielectric characterization of liquids [44] (other planar sensors combined with microfluidic's technology, either operating in reflection or transmission, have been reported [45]–[53]). Recently, highly sensitive reflective-mode phase-

This work was supported by MCIN/AEI 10.13039/501100011033, Spain, through the projects PID2019-103904RB-I00 (ERDF European Union) and PDC2021-121085-I00 (European Union Next Generation EU/PRTR), by the AGAUR Research Agency, Catalonia Government, through the project 2017SGR-1159, and by Institució Catalana de Recerca i Estudis Avançats (who awarded Ferran Martín). P. Casacuberta acknowledges the Ministerio de Universidades, Spain, for the FPU grant (Ayudas para la formación de profesorado universitario), ref. FPU20/05700. J. Muñoz-Enano acknowledges Secreteraria d'Universitats i Recerca (Gen. Cat.) and European Social Fund for the FI grant. Lijuan Su acknowledges the Juan de la Cierva Program for the support through the project IJC2019-040786-I.

P. Casacuberta, P. Vélez, J. Muñoz-Enano, L. Su, and F. Martín are with GEMMA/CIMITEC, Departament d'Enginyeria Electrònica, Universitat Autònoma de Barcelona, 08193 Bellaterra, Spain.
E-mail: Ferran.Martin@uab.es.

variation permittivity sensors have been proposed [6]. Such sensors are implemented by means of either a high-impedance quarter-wavelength or a low-impedance half-wavelength open-ended sensing line, cascaded to a set of 90° lines with alternating high and low characteristic impedance. As it was demonstrated in [6], the impedance contrast of the high/low-impedance 90° lines generates a multiplicative effect on the sensitivity, with the result of extremely competitive sensors, able to detect and resolve tiny variations in the dielectric constant of the MUT in the vicinity of a certain (design) value. The figure of merit (FoM) of these sensors, defined as the ratio between the maximum sensitivity and the area of the sensing region expressed in terms of the squared guided wavelength, is also very good. However, the requirement of an extra region, i.e., the step-impedance line, to boost up the sensitivity represents a penalty in terms of the overall sensor size.

In this paper, we propose a new type of reflective-mode phase-variation sensors exhibiting very high, and controllable, sensitivity and compact size, devoted to dielectric characterization. The sensors, one-port devices, merely consist of a pair of coupled lines (the sensing region) with an adequate termination, and the sensitivity can be significantly enhanced by setting the electrical length of the line pair to the adequate value (90°), and by weakly coupling the lines. By this means, sensitivity optimization does not require further circuit stages, contrary to the sensors reported in [6]–[8], [12], [13], [16]. It should be mentioned that other sensors exploiting electromagnetic coupling between resonant elements for sensitivity enhancement have been reported [53]–[56]. There are also various sensors based on coupled lines available in the literature [57]–[61], but their working principle is radically different to the one reported in this paper.

The work is organized as follows. The topology of the sensing structure, as well as the sensing approach, including the potential for sensitivity optimization, are included in Section II. Section III reports the working principle and a detailed analysis devoted to obtain the optimum conditions for sensitivity optimization. Then this analysis is applied to the design of three prototype sensors, which are validated by simulation and experimentally in Section IV. Section V analyzes the effects of losses. The purpose of this section is to demonstrate that, under the low-loss approximation, the output variable does not significantly vary, and to quantify the limits of such approximation. The proposed sensors are compared to other phase-variation sensors in Section VI. Finally, the main conclusions of the work are highlighted in Section VII.

II. The Proposed Coupled-Line-Based Sensor

The proposed permittivity sensor consists of a pair of coupled lines where three of the four ports (designated as 2, 3 and 4) are terminated either by a short- or by an open-circuit, whereas port 1 acts as the input port (Fig. 1). The device is thus a one-port reflective-mode sensor, and the sensing area (indicated by a dashed rectangle in Fig. 1) is delimited by the extension occupied by the coupled lines, plus a certain lateral margin, 10 mm per side in this case.

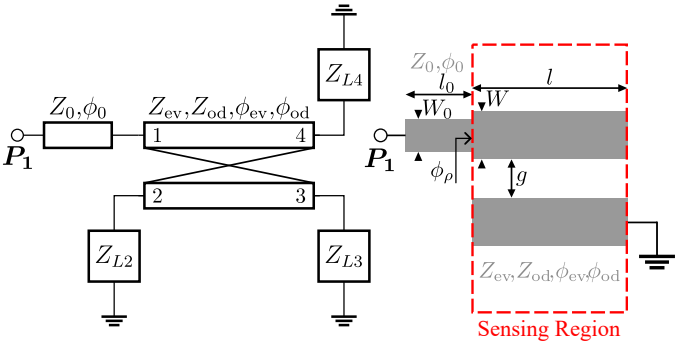

Fig. 1. Schematic (left side) and layout (right side) of the proposed coupled-line-based sensor and relevant electrical and geometrical parameters. The port terminations, Z_{L2}, Z_{L3},Z_{L4}, are either an open- or a short-circuit. In the specific layout, the termination of port 3 is a short-circuit, wheras ports 2 and 4 are left open-circuited (corresponding to Sensor-type A, that will be discussed later). The line section outside the sensing region, characterized by the width W_0 and length l_0, is the access line.

The output variable is the phase of the reflection coefficient, an easily measurable quantity, whereas the input variable is the dielectric constant of the MUT, placed on top of the sensing region. The coupled lines are characterized by the even- and odd-mode characteristic impedances, $Z_{\rm ev}$ and $Z_{\rm od}$, respectively, and by the even- and odd-mode electrical lengths, $\phi_{\rm ev}$ and $\phi_{\rm od}$.

The working principle of these sensors is similar to the one of reflective-mode phase-variation sensors based on open-ended sensing lines [6]–[8]. Namely, the dielectric constant of the MUT has direct influence on the electrical length, or phase, and characteristic impedance of the open-ended sensing line, which in turn determine the phase of the reflection coefficient. It was demonstrated in [6] that sensitivity optimization in these sensors is achieved by implementing the open-ended sensing line by means of either a low-impedance 180° line section, or a high-impedance 90° line section. In practice, the sensitivity is limited by the achievable impedance (high or low) of the sensing line, but the sensitivity can be further enhanced by cascading 90° line sections with alternating high and low characteristic impedance (step impedance line). This does not represent an increase of the sensing region, but enlarges the overall size of the sensor.

In this paper, the idea is to investigate the possibility of enhancing the sensitivity, avoiding the use of the step-impedance structure composed of 90° line sections, by adding a line coupled to the main (sensing) line of the sensor. The degrees of freedom of the resulting coupled line pair are thus incremented, as compared to the sensor based merely on an open-ended sensing line, and, potentially, the sensitivity can be enhanced, as it will be demonstrated. For sensitivity optimization, the necessary terminations of the coupled lines, as well as the electrical lengths and characteristic impedances for both modes (even and odd) and the coupling factor, must be determined (to be discussed in the next section).

III. Working Principle and Sensitivity Analysis

In [6], sensitivity enhancement was achieved by tuning the operating frequency of the sensor to the one providing

an electrical length of either 90° or 180° to the open-ended sensing line. In the former case, the sensing line behaves as a grounded series resonator, the phase variation of the reflection coefficient is maximum at resonance, and such variation increases with the characteristic impedance of the sensing line (equivalent to a large phase variation in a high-Q series resonator). For a 180° open-ended sensing line, the open-ended termination is translated to the input port, and thereby the line resembles a grounded parallel resonator. In this case, however, for sensitivity optimization, the characteristic impedance of the line must be low (corresponding to a high-Q parallel resonator). The maximum achievable sensitivity is limited by the maximum and minimum characteristic impedance of the 90° and 180° sensing lines, respectively. For that reason, a step-impedance line, generating a multiplicative effect on the sensitivity, was cascaded to the 90° or 180° open-ended sensing lines in the sensors of [6].

In the sensors reported in this work, the strategy for enhancing the sensitivity consists in coupling a resonant element, implemented by means of a quarter-wavelength transmission line resonator, to the main sensing line, also based on a quarter-wavelength resonator. Due to electromagnetic coupling, the resonance frequency of the isolated resonator splits into two frequencies, separated a distance that depends on the coupling factor. By weakly coupling the resonant elements, or, more precisely, the coupled lines, it is thus expected that the resonance frequencies are closely spaced. Since the phase between two consecutive resonances must experience an excursion of 360°, assuming that losses are negligible (a reasonable approximation), it follows that, by weakly coupling the lines, the sensitivity can (potentially) be enhanced substantially (the scheme of this sensitivity enhancement strategy is depicted in Fig. 2). Obviously, sensitivity optimization can be achieved for the dielectric constant of the MUT providing an electrical length of a quarter-wavelength to the coupled lines at the operating frequency (this MUT is designated as reference –REF– material). Note that, in this analysis, it is indeed considered that the coupled lines exhibit identical phase for the even and odd modes, which is not strictly true in open coupled lines (e.g., microstrip or coplanar waveguides, CPW), such as those that are required for material sensing [62]. Nevertheless, for weakly coupled lines, it is reasonable to consider that $\phi_{\rm ev} = \phi_{\rm od}$, at least for the purpose of conceptually justifying the sensing enhancement approach.

In order to calculate the sensitivity of the proposed sensing structure, defined as the variation of the phase of the reflection coefficient with the dielectric constant of the MUT, it is first necessary to calculate the impedance seen from the input port. For that purpose, the order-4 impedance matrix, $\mathbf{Z}$, of the coupled lines is used. The elements of this matrix for $\phi_{\rm ev} = \phi_{\rm od}$ are provided in [62], but generalization to the case where this condition is not satisfied is simple (as seen in [63]). The following results are obtained

$$Z_{11} = Z_{22} = Z_{33} = Z_{44} = -\frac{j}{2}\left\{Z_{\rm ev}\cot\phi_{\rm ev} + Z_{\rm od}\cot\phi_{\rm od}\right\} \tag{1a}$$

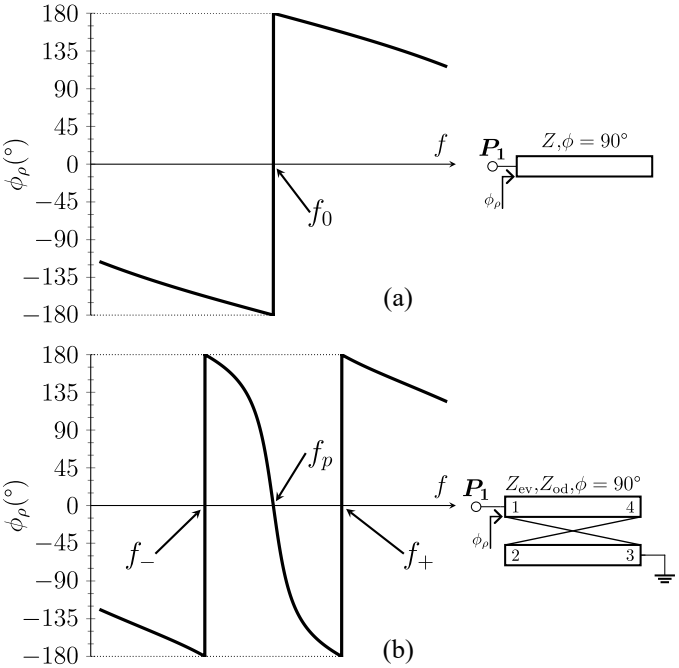

Fig. 2. Sketch showing the enhancement of the variation in the phase of the reflection coefficient of a quarter-wavelength resonator weakly coupled to an identical resonator (the specific sketch corresponds to Sensor-type A, as described later in the text). Note that $f_p = f_0$. On the left side, the phase of the reflection coefficient seen from the input port, and on the right side the schematic representation. The isolated quarter-wavelength resonator case depicted in (a), and in (b), the weakly coupled resonators case.

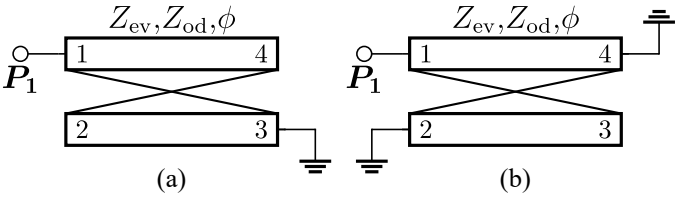

Fig. 3. Port terminations for sensor A (a) and sensor B (b).

$$Z_{12} = Z_{21} = Z_{34} = Z_{43} = -\frac{j}{2}\left\{Z_{\rm ev}\cot\phi_{\rm ev} - Z_{\rm od}\cot\phi_{\rm od}\right\} \tag{1b}$$

$$Z_{13} = Z_{31} = Z_{24} = Z_{42} = -\frac{j}{2}\left\{Z_{\rm ev}\frac{1}{\sin\phi_{\rm ev}} - Z_{\rm od}\frac{1}{\sin\phi_{\rm od}}\right\} \tag{1c}$$

$$Z_{14} = Z_{41} = Z_{23} = Z_{32} = -\frac{j}{2}\left\{Z_{\rm ev}\frac{1}{\sin\phi_{\rm ev}} + Z_{\rm od}\frac{1}{\sin\phi_{\rm od}}\right\} \tag{1d}$$

Let us now consider two specific sensing structures based on quarter-wavelength coupled lines, with the terminations indicated in Fig. 3, and corresponding to coupled resonators. For the structure designated as Sensor A, the input impedance can be expressed in terms of the elements of the impedance matrix as

$$Z_{{\rm in},A} = Z_{11} - \frac{Z_{13}^2}{Z_{11}} \tag{2}$$

whereas for sensor B, the input impedance is found to be

$$Z_{{\rm in},B} = Z_{11} - \frac{Z_{11}\left({Z_{12}}^2 + {Z_{14}}^2\right) - 2Z_{12}Z_{13}Z_{14}}{{Z_{11}}^2 - {Z_{13}}^2} \tag{3}$$

Let us first analyze sensor A. Introduction of the elements of the impedance matrix (1) in (2) gives

$$Z_{\mathrm{in},A} = -\frac{j}{2}\frac{2Z_{\mathrm{ev}}Z_{\mathrm{od}}(\cos\phi_{\mathrm{ev}}\cos\phi_{\mathrm{od}}+1)-(Z_{\mathrm{ev}}^2+Z_{\mathrm{od}}^2)\sin\phi_{\mathrm{ev}}\sin\phi_{\mathrm{od}}}{Z_{\mathrm{ev}}\cos\phi_{\mathrm{ev}}\sin\phi_{\mathrm{od}}+Z_{\mathrm{od}}\cos\phi_{\mathrm{od}}\sin\phi_{\mathrm{ev}}} \tag{4}$$

Inspection of (4) reveals that for sufficiently separated lines, i.e., with negligible coupling, the impedances and phases for both modes are identical, and the input impedance is the one of an open-ended line with impedance $Z = Z_{\mathrm{ev}} = Z_{\mathrm{od}}$ and electrical length $\phi = \phi_{\mathrm{ev}} = \phi_{\mathrm{od}}$, i.e.,

$$Z_{\mathrm{in},A} = -jZ\cot\phi \tag{5}$$

as expected. Thus, the input impedance is null for $\phi = 90°$ and odd multiples (the behavior of the line is similar to that of a grounded series resonator in the vicinity of the frequency providing such phase conditions). For finite coupling, the zeros of (4) provide the resonance frequencies, and it is apparent that for weak coupling two solutions close to the fundamental resonance frequency of the isolated line (the one giving $\phi = 90°$) are obtained. Indeed, for very weak coupling, it is reasonable to consider that $\phi_{\mathrm{ev}} \approx \phi_{\mathrm{od}} = \phi$, and expression (4) simplifies to

$$Z_{\mathrm{in},A} = -j\frac{2Z_{\mathrm{ev}}Z_{\mathrm{od}}(\cos^2\phi+1)-(Z_{\mathrm{ev}}^2+Z_{\mathrm{od}}^2)\sin^2\phi}{2(Z_{\mathrm{ev}}+Z_{\mathrm{od}})\cos\phi\sin\phi} \equiv j\chi_{\mathrm{in},A} \tag{6}$$

where $\chi_{\mathrm{in},A}$ is the input reactance. Expression (6) is also valid under moderate coupling provided the REF material exhibits a dielectric constant identical to the one of the substrate. The zeros of (6) are given by the solutions of

$$\cos\phi = \pm\frac{Z_{\mathrm{ev}}-Z_{\mathrm{od}}}{Z_{\mathrm{ev}}+Z_{\mathrm{od}}} \equiv \pm C \tag{7}$$

and are controlled by the coupling factor, C. When the coupling vanishes ($C \to 0$), the two solutions, designated as ϕ_+ and ϕ_-, merge in a single resonance frequency corresponding to $\phi = 90°$. From (7), it follows that the two zeros, f_+ and f_- (present at both sides of the resonance frequency of the isolated quarter-wavelength resonator), can be as closely spaced as desired, by simply weakly coupling the lines. It is also interesting to mention that for the frequency satisfying $\phi = 90°$, the denominator of (6) vanishes, whereas the numerator is finite (provided $Z_{\mathrm{ev}} \neq Z_{\mathrm{od}}$). Consequently, the input impedance, $Z_{\mathrm{in},A}$, exhibits a pole at that frequency, f_p (see Fig. 2).

According to the previous paragraph, a significant variation of the phase of the reflection coefficient is achievable in the vicinity of the pole frequency by weakly coupling the lines. The reason is that the reflection coefficient is $\rho = -1$ and $\rho = +1$ at the zero and pole frequencies, respectively. Thus, the phase of the reflection coefficient should experience an excursion of 360° between two closely spaced frequencies (f_+ and f_-), provided the phase of the reflection coefficient is $\phi_\rho = \pm 180°$ at f_+ and f_- (or ϕ_+ and ϕ_-), and it is $\phi_\rho = 0°$ at f_p (or $\phi = 90°$). Note that the phase of the reflection coefficient is a decreasing function with frequency.

For Sensor B, expression (3), using the matrix elements of (1), gives

$$Z_{\mathrm{in},B} = j\frac{2Z_{\mathrm{ev}}Z_{\mathrm{od}}(Z_{\mathrm{ev}}\cot\phi_{\mathrm{od}}+Z_{\mathrm{od}}\cot\phi_{\mathrm{ev}})\sin\phi_{\mathrm{ev}}\sin\phi_{\mathrm{od}}}{2Z_{\mathrm{ev}}Z_{\mathrm{od}}(\cos\phi_{\mathrm{ev}}\cos\phi_{\mathrm{od}}+1)-(Z_{\mathrm{ev}}^2+Z_{\mathrm{od}}^2)\sin\phi_{\mathrm{ev}}\sin\phi_{\mathrm{od}}} \tag{8}$$

and for very weakly coupled lines, or for a REF material identical to the one of the substrate, with $\phi_{\mathrm{ev}} \approx \phi_{\mathrm{od}} = \phi$, expression (8) simplifies to

$$Z_{\mathrm{in},B} = j\frac{2Z_{\mathrm{ev}}Z_{\mathrm{od}}(Z_{\mathrm{ev}}+Z_{\mathrm{od}})\cos\phi\sin\phi}{2Z_{\mathrm{ev}}Z_{\mathrm{od}}(\cos^2\phi+1)-(Z_{\mathrm{ev}}^2+Z_{\mathrm{od}}^2)\sin^2\phi} \equiv j\chi_{\mathrm{in},B} \tag{9}$$

If the coupling is null ($Z_{\mathrm{ev}} = Z_{\mathrm{od}} = Z$), the input impedance is found to be

$$Z_{\mathrm{in},B} = jZ\tan\phi \tag{10}$$

corresponding to the impedance of a line with a short-circuit termination. Such line behaves as a grounded parallel resonator in the vicinity of the frequency providing a phase of $\phi = 90°$, where $Z_{\mathrm{in},B} = \infty$. However, when coupling is activated ($Z_{\mathrm{ev}} \neq Z_{\mathrm{od}}$), the numerator of (9) nulls for $\phi = 90°$, whereas the denominator is finite, which means that there is a zero at that frequency, f_z. At both sides of such frequency, two poles arise as consequence of coupling. Such poles are given by the two frequencies, f_+ and f_-, that null the denominator of (9), corresponding to the phases, ϕ_+ and ϕ_-, which are the solutions of equation (7). The difference with regard to sensor A is that, at the frequencies f_+ and f_-, an open-circuit, rather than a short-circuit, is seen from the input port of the coupled lines. For sensor B, the phase of the reflection coefficient is $\phi_\rho = 0°$ at f_+ and f_- (or ϕ_+ and ϕ_-), and it is $\phi_\rho = \pm 180°$ at f_z (or $\phi = 90°$). Thus, an identical excursion of the unwrapped phase (360°) is expected for frequencies varying between f_+ and f_-.

Under the weak coupling approximation or for a REF material with dielectric constant identical to the one of the substrate ($\phi_{\mathrm{ev}} \approx \phi_{\mathrm{od}} = \phi$), the sensitivity, or derivative of the phase of the reflection coefficient, ϕ_ρ, with the dielectric constant of the MUT, $\varepsilon_{\mathrm{MUT}}$, for both sensors can be written as

$$S = \frac{d\phi_\rho}{d\varepsilon_{\mathrm{MUT}}} = \frac{d\phi_\rho}{d\phi}\frac{d\phi}{d\varepsilon_{\mathrm{MUT}}} + \frac{d\phi_\rho}{dZ_{\mathrm{ev}}}\frac{dZ_{\mathrm{ev}}}{d\varepsilon_{\mathrm{MUT}}} + \frac{d\phi_\rho}{dZ_{\mathrm{od}}}\frac{dZ_{\mathrm{od}}}{d\varepsilon_{\mathrm{MUT}}} \tag{11}$$

where the reflection coefficient and the phase of the reflection coefficient are given by

$$\rho = \frac{Z_{\mathrm{in}}-Z_0}{Z_{\mathrm{in}}+Z_0} = \frac{j\chi_{\mathrm{in}}-Z_0}{j\chi_{\mathrm{in}}+Z_0} \tag{12}$$

and

$$\phi_\rho = 2\arctan\left(-\frac{\chi_{\mathrm{in}}}{Z_0}\right) \tag{13}$$

respectively, where $\chi_{\mathrm{in}} = \chi_{\mathrm{in},A}$ for sensor A, $\chi_{\mathrm{in}} = \chi_{\mathrm{in},B}$ for sensor B, and Z_0 is the reference impedance of the ports ($Z_0 = 50\ \Omega$ in this work).

Let us now calculate the sensitivity for $\phi = 90°$, corresponding to f_p for sensor A and to f_z for sensor B, i.e., the intermediate frequency in the range between f_+ and f_- for each sensor. Indeed, the last two terms of the right-hand side member of (11) evaluated at $\phi = 90°$ are null for both sensors, since $d\phi_\rho/dZ_{\mathrm{ev}} = d\phi_\rho/dZ_{\mathrm{od}} = 0$ for such phase condition. Concerning the first term, the key derivative is the first one. For arbitrary values of ϕ, such derivative is given by

$$\frac{d\phi_\rho}{d\phi} = -4Z_0\frac{(Z_{\mathrm{ev}}+Z_{\mathrm{od}})^3\cos^2\phi+(Z_{\mathrm{ev}}+Z_{\mathrm{od}})(Z_{\mathrm{ev}}-Z_{\mathrm{od}})^2\left(\sin^2\phi-\cos^2\phi\right)}{4Z_0^2(Z_{\mathrm{ev}}+Z_{\mathrm{od}})^2\sin^2\phi\cos^2\phi+[(Z_{\mathrm{ev}}+Z_{\mathrm{od}})^2\cos^2\phi-(Z_{\mathrm{ev}}-Z_{\mathrm{od}})^2]^2} \tag{14}$$

for sensor A, and

$$\frac{d\phi_\rho}{d\phi} = -4Z_0 Z_{\rm ev} Z_{\rm od} \frac{(Z_{\rm ev}+Z_{\rm od})^3\cos^2\phi-(Z_{\rm ev}+Z_{\rm od})(Z_{\rm ev}-Z_{\rm od})^2\left(\sin^2\phi-\cos^2\phi\right)}{4Z_{\rm ev}^2 Z_{\rm od}^2(Z_{\rm ev}+Z_{\rm od})^2\sin^2\phi\cos^2\phi+Z_0^2[(Z_{\rm ev}+Z_{\rm od})^2\cos^2\phi-(Z_{\rm ev}-Z_{\rm od})^2]^2} \tag{15}$$

for sensor B. Evaluation of (14) and (15) for $\phi = 90°$ gives

$$\left.\frac{d\phi_\rho}{d\phi}\right|_{A,\phi=90°} = -4Z_0\frac{Z_{\rm ev}+Z_{\rm od}}{(Z_{\rm ev}-Z_{\rm od})^2} = \frac{-4Z_0}{C^2(Z_{\rm ev}+Z_{\rm od})} \tag{16}$$

for sensor A, and

$$\left.\frac{d\phi_\rho}{d\phi}\right|_{B,\phi=90°} = -4\frac{Z_{\rm ev}Z_{\rm od}}{Z_0}\frac{Z_{\rm ev}+Z_{\rm od}}{(Z_{\rm ev}-Z_{\rm od})^2} = \frac{-4Y_0}{C^2(Y_{\rm ev}+Y_{\rm od})} \tag{17}$$

for sensor B, with $Y_{\rm ev} = 1/Z_{\rm ev}$, $Y_{\rm od} = 1/Z_{\rm od}$ and $Y_0 = 1/Z_0$.

It is apparent from (16) and (17) that, for sensitivity optimization in the vicinity of the dielectric constant of the REF material (where $\phi = 90°$), the coupling factor must be as small as possible. Since the dependence with such term is quadratic, it is potentially possible to achieve very high sensitivity by weakly coupling the lines. Nevertheless, there is a limit, since extremely weak coupling is not expected to provide an unlimited sensitivity. The reason is that losses prevent that the phase excursion between f_+ and f_- is 360°, when the coupling is extremely weak. Moreover, for extremely weak coupling, the separation between f_+ and f_- is so small that it is not possible to tune in practice the sensor to the required frequency value, f_0. On the other hand, low even and odd mode impedances for sensor A, and high even and odd mode impedances for sensor B, contribute to enhance the terms (16) and (17) of the sensitivity. Note that, according to (11), the whole sensitivity depends also on the derivative of the electrical length with the dielectric constant of the MUT, $d\phi/d\varepsilon_{\rm MUT}$. Nevertheless, previous to calculate the contribution of such term, let us validate the effects of the coupling factor and impedances (even and odd) of the coupled lines on the sensitivity. For that purpose, we have considered the schematic of both sensors, A and B, and we have set the phase of the coupled lines to $\phi = 90°$ (ideal coupled lines, with identical phase for both modes, are considered). Then we have varied the phase of the coupled lines in the vicinity of that value, and we have obtained the phase of the reflection coefficient with the *Keysight ADS* circuit simulator (Fig. 4). The different curves for both sensors correspond to various combinations of $Z_{\rm ev}$ and $Z_{\rm od}$ (such values, as well as the corresponding coupling factors, are indicated in the figure). From those curves, the corresponding sensitivities $d\phi_\rho/d\phi$ are obtained (also depicted in Fig. 4). As expected, the sensitivity is a maximum at $\phi = 90°$ for each combination of $Z_{\rm ev}$ and $Z_{\rm od}$, and the value is in perfect agreement with the predictions of (16) and (17). Thus, the strong influence of C on the sensitivity is confirmed. It is also demonstrated that for sensitivity enhancement the impedances should be low for sensor A, and high for sensor B.

With regard to the derivative of the phase of the coupled lines with the dielectric constant of the MUT, $d\phi/d\varepsilon_{\rm MUT}$, within the weak coupling approximation, it is reasonable to consider that the dependence of ϕ with $\varepsilon_{\rm MUT}$ is that of an

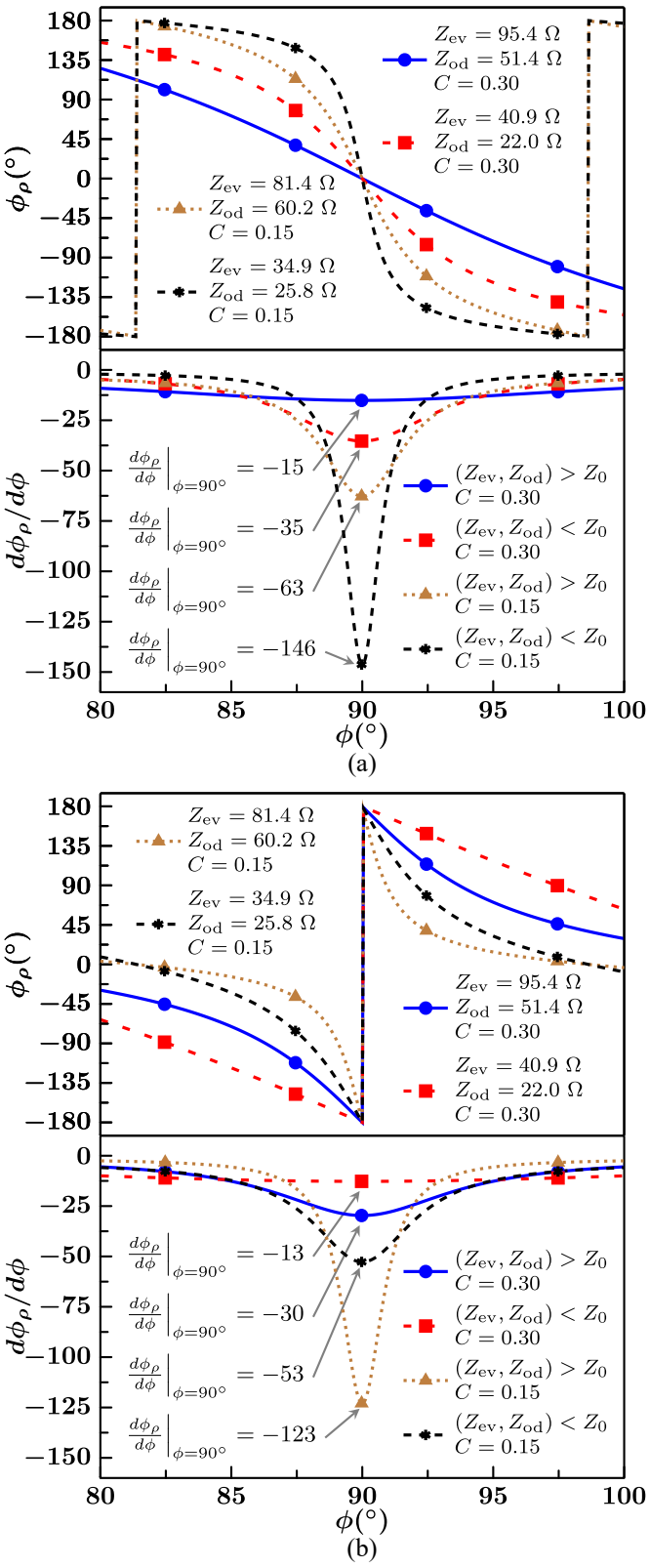

Fig. 4. Phase of the reflection coefficient, ϕ_ρ, as a function of the electrical length of the pair of coupled lines, ϕ, and sensitivity ($d\phi_\rho/d\phi$) for sensor A (a) and for sensor B (b). The different combinations of characteristic impedances for the even- and odd-modes are indicated.

isolated line with identical width, i.e.,

$$\phi = \frac{\omega_0 l}{c}\sqrt{\varepsilon_{\rm eff}} \tag{18}$$

where c is the speed of light in vacuum, l is the length of the line, and the effective dielectric constant is (microstrip technology is considered) [62]

$$\varepsilon_{\rm eff} = \frac{\varepsilon_r + \varepsilon_{\rm MUT}}{2} + \frac{\varepsilon_r - \varepsilon_{\rm MUT}}{2} F \tag{19}$$

where ε_r is the dielectric constant of the substrate and F is a geometry factor given by

$$F = \left(1 + 12\frac{h}{W}\right)^{-\frac{1}{2}} \tag{20a}$$

for $W/h \geq 1$, or by

$$F = \left(1 + 12\frac{h}{W}\right)^{-\frac{1}{2}} + 0.04\left(1 - \frac{W}{h}\right)^2 \tag{20b}$$

for $W/h < 1$. In (20), h and W are the substrate thickness and the width of the coupled lines, respectively, and it is assumed that $t \ll h$, where t is the thickness of the metallic layer. It should be mentioned that the validity of (19) is subjected to the fact that the MUT is thick enough, so that the electromagnetic field generated by the coupled lines does not reach the MUT-air interface (i.e., this means that the MUT can be considered to be semi-infinite in the vertical direction). Using (18) and (19), the derivative of the phase of the coupled lines with the dielectric constant of the MUT is found to be

$$\frac{d\phi}{d\varepsilon_{\rm MUT}} = \frac{\omega_0 l(1-F)}{4c\sqrt{\varepsilon_{\rm eff}}} = \frac{\phi(1-F)}{4\varepsilon_{\rm eff}} \tag{21}$$

Thus, the overall sensitivity, as given by (11), for $\varepsilon_{\rm MUT}$ corresponding to the dielectric constant of the REF material, $\varepsilon_{\rm REF}$, and the sensor designed to exhibit a phase of $\phi = 90°$ when the line pair is covered with such material, is

$$S = \left.\frac{d\phi_\rho}{d\varepsilon_{\rm MUT}}\right|_{A,\varepsilon_{\rm MUT}=\varepsilon_{\rm REF}} = \frac{-Z_0\pi(1-F)}{2C^2(Z_{\rm ev}+Z_{\rm od})\varepsilon_{\rm eff,REF}} \tag{22}$$

for sensor A, and

$$S = \left.\frac{d\phi_\rho}{d\varepsilon_{\rm MUT}}\right|_{B,\varepsilon_{\rm MUT}=\varepsilon_{\rm REF}} = \frac{-Y_0\pi(1-F)}{2C^2(Y_{\rm ev}+Y_{\rm od})\varepsilon_{\rm eff,REF}} \tag{23}$$

for sensor B. To infer (22) and (23), expressions (16) and (17) have been used, and $\varepsilon_{\rm eff,REF}$ is the effective dielectric constant, given by (19), when the line pair is covered with the REF material (i.e., $\varepsilon_{\rm MUT} = \varepsilon_{\rm REF}$). Expressions (22) and (23) can be used for sensor design, as far as such equations provide a link between the sensitivity for the REF material, the main relevant parameter, and the electrical and geometrical parameters of the coupled lines. Note that if the dielectric constant of the REF material is identical to the one of the substrate, the weak coupling approximating is not necessary, and expressions (22) and (23) are valid by replacing $\varepsilon_{\rm eff,REF}$ with ε_r.

As it will be shown in Section IV, focused on experimental validation by considering three different prototypes, the weak coupling approximation, expressions (22) and (23) in the limit of small perturbations, provides a reasonable prediction of the maximum sensitivity (the one corresponding to $\varepsilon_{\rm MUT} = \varepsilon_{\rm REF}$). The reason is that the considered coupling levels are low and/or the dielectric constant of the REF material coincides with the one of the substrate. Nevertheless, if the weak coupling approximation is not valid, and the REF material does not coincide with that of the substrate, the assumption $\phi_{\rm ev} \approx \phi_{\rm od} = \phi$ cannot be applied. Under these conditions, the sensitivity should be expressed as:

$$S = \frac{d\phi_\rho}{d\varepsilon_{\rm MUT}} = \frac{d\phi_\rho}{d\phi_{\rm ev}}\frac{d\phi_{\rm ev}}{d\varepsilon_{\rm MUT}} + \frac{d\phi_\rho}{d\phi_{\rm od}}\frac{d\phi_{\rm od}}{d\varepsilon_{\rm MUT}} + \frac{d\phi_\rho}{dZ_{\rm ev}}\frac{dZ_{\rm ev}}{d\varepsilon_{\rm MUT}} + \frac{d\phi_\rho}{dZ_{\rm od}}\frac{dZ_{\rm od}}{d\varepsilon_{\rm MUT}} \tag{24}$$

The analytical calculation of the sensitivity is not simple in this case, but it can be calculated numerically (however, this is out of the scope of this paper). Let us mention that the proposed sensors are specially suited to achieve high sensitivities, and this requires weak couplings. Thus, the considered weak coupling approximation, applied in this work, is justified.

IV. Sensor Validation

For sensor validation, we have designed and fabricated one prototype device of sensor type A and two prototype devices of sensor type B. The operating frequency is set in all the cases to $f_0 = 2$ GHz and the considered substrate is the *Rogers RO4003C* with dielectric constant $\varepsilon_r = 3.55$ and thickness $h = 1.524$ mm. The loss tangent of this substrate is $\tan\delta = 0.0022$.

A. Sensor type A with moderate coupling and $\varepsilon_{\rm REF} = \varepsilon_r = 3.55$

For the designed sensor A, the transverse geometry of the coupled lines is the one corresponding to an even- and odd mode impedances of $Z_{\rm ev} = 42.7\ \Omega$ and $Z_{\rm od} = 22.8\ \Omega$, respectively, when the REF material is identical to the one of the substrate (i.e., the coupled lines are covered by means of a semi-infinite material with dielectric constant $\varepsilon_{\rm REF} = \varepsilon_r = 3.55$). With such even and odd mode impedances, the coupling coefficient is $C = 0.30$, corresponding to a moderate (not weak) value. Nevertheless, since the dielectric constant of the REF material is identical to the one of the substrate, it can be assumed that for small variations of the dielectric constant of the MUT in the vicinity of $\varepsilon_{\rm REF}$, the phases satisfy $\phi_{\rm ev} \approx \phi_{\rm od} = \phi$, and hence the analysis of the previous section can be considered to be valid. The photograph of this sensor, fabricated by means of a *LPKF H100* drilling machine, is depicted in Fig. 5(a). Short circuiting the required terminations of the coupled lines has been carried out by means of vias. For connector soldering, 50-Ω access lines have been cascaded to the input port of the coupled lines.

Previous to the experimental validation, we have first obtained the phase of the simulated reflection coefficient at f_0 as a function of the dielectric constant of the MUT by means of electromagnetic simulation (the *CST Studio Suite* commercial software has been used for that purpose). The considered thickness of the MUT has been set to 18.3 mm, corresponding to a stacking of 12 samples of 1.524 mm, available in our laboratory for different dielectric constants. Such thickness is

enough to contemplate the semi-infinite MUT approximation. The considered input dynamic range is the interval between $\varepsilon_{\rm MUT} = 1$ and $\varepsilon_{\rm MUT} = 12$, and the dielectric constant step between adjacent simulations has been set to 0.5, except between $\varepsilon_{\rm MUT} = 3$ and $\varepsilon_{\rm MUT} = 4$, which has been set to 0.05. With this increase in the density of data points in the vicinity of $\varepsilon_{\rm REF}$, the sensitivity can be more accurately calculated. The phase variation, $\Delta\phi_\rho$, with $\varepsilon_{\rm MUT}$, and the sensitivity are depicted in Fig. 5(b), where $\Delta\phi_\rho = \phi_\rho - \phi_{\rho,\varepsilon_{\rm REF}}$ ($\phi_{\rho,\varepsilon_{\rm REF}}$ is the phase of the reflection coefficient when the MUT is the REF material). The sensitivity for $\varepsilon_{\rm MUT} = \varepsilon_{\rm REF}$, inferred from the simulated data points, is indicated in the figure. The value is in reasonable good agreement with the predictions of expression (22).

Experimental validation has been carried out by considering samples of different dielectric constant, in particular uncladded commercially available substrates and Fused Deposition Modeling (FDM) 3D printed PLA (fabricated with the *Ultimaker 3 Extended* printer). The specific dielectric constants are 2.7 (estimated for PLA), 3.55 (for *Rogers RO4003C*), 4.4 (for *FR4*), and 10.2 (for *Rogers RO3010*). As indicated before, 12 pieces of roughly 1.5 mm have been stacked in each case, or directly 3D printed in the case of PLA. The area of the samples is identical to the one indicated by the dashed rectangle in Fig. 5(a). The phase of the reflection coefficient at f_0 has been measured by means of a vector network analyzer (model *Keysight N5221A*). In order to avoid the well-known effects of the air gap, potentially present between the MUT and the sensor substrate, we have pressured the MUTs against the sensor by means of nylon screws. The measured data points are also included in Fig. 5(b), and show good agreement with the simulated values. It should be mentioned that, in order to ensure repetitiveness of the results, three independent measurement have been performed for each sample (thus, the mean value plus the error bars are included in Fig. 5).

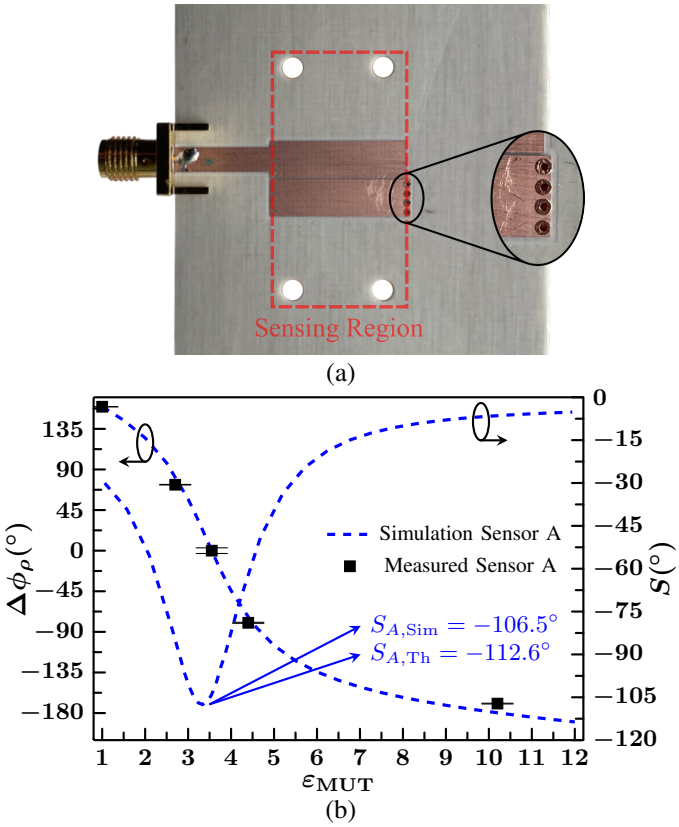

Fig. 5. Photograph of the fabricated sensor A (a) and phase of the reflection coefficient at f_0 by varying the dielectric constant of the MUT and sensitivity (b). The sensing region is indicated with a dashed rectangle. Dimensions (in mm) are: $W = 5$, $g = 0.2$ and $l = 18.32$. The dimensions of the 50-Ω access lines (in mm) are: $W_0 = 3.33$, $l_0 = 12.8$.

B. Sensor type B with weak coupling and $\varepsilon_{\rm REF} = \varepsilon_r = 3.55$

The first prototype device of sensor type B (designated as Sensor B) exhibits weak coupling and the REF material is identical to the substrate ($\varepsilon_{\rm REF} = \varepsilon_r = 3.55$). For the prototype presented in this subsection, the even and odd mode impedances have been set to $Z_{\rm ev} = 92.2\ \Omega$ and $Z_{\rm od} = 68.3\ \Omega$, respectively, providing a coupling level of $C = 0.15$. The photograph of this sensor prototype is depicted in Fig. 6(a). The simulated phase of the reflection coefficient, $\Delta\phi_\rho$, at f_0 as a function of the dielectric constant of the MUT is shown in Fig. 6(b). Similar to Sensor A, the thickness of the MUT has been set to 18.3 mm, and the input dynamic range is also identical, i.e., between $\varepsilon_{\rm MUT} = 1$ and $\varepsilon_{\rm MUT} = 12$. The sensitivity inferred from the simulated phase points is also included in Fig. 6(b). The value of the sensitivity for $\varepsilon_{\rm MUT} = \varepsilon_{\rm REF}$ has been found to be $-659.6°$, i.e., in good agreement with the theoretical prediction using expression (23). This is a high sensitivity, inferred by virtue of the relatively weak coupling between the coupled lines. Indeed, as compared to the reflective-mode sensors based on a single open-ended 90°or 180°lines [6], the sensitivity is improved by a factor of roughly C^{-2}. Thus, it is demonstrated that the use of coupled lines is a good strategy for sensitivity enhancement. In [6]–[8], very good sensitivities were obtained in the reported sensors, but at the expense of cascading high/low impedance 90°line sections to the 90°, or 180°, open-ended sensing lines. The experimental data points, corresponding to the measured phases of the reflection coefficient inferred by means of identical samples to those used for the experimental validation of Sensor A, are also depicted in Fig. 6(b), where it can be appreciated that the agreement is also good.

For this sensor, a different set of simulations and experiments has been carried out. Particularly, we have inferred the phase of the reflection coefficient by varying the number of stacked samples, considering that the dielectric constant of such samples is the one of the REF sample, i.e., 3.55. The effect is a variation of the equivalent dielectric constant of the MUT. The simulated and measured data points are depicted in Fig. 7, where, again, good agreement between the simulated and measured data has been obtained. Note that there is a quasi-saturation effect in the results shown in Fig. 7, as corresponds to the fact that when the number of stacked samples increases, the overall MUT thickness approaches the one required for the consideration of a semi-infinite MUT. Above such value, no longer variation in the phase of the reflection coefficient is expected, since the field lines do not

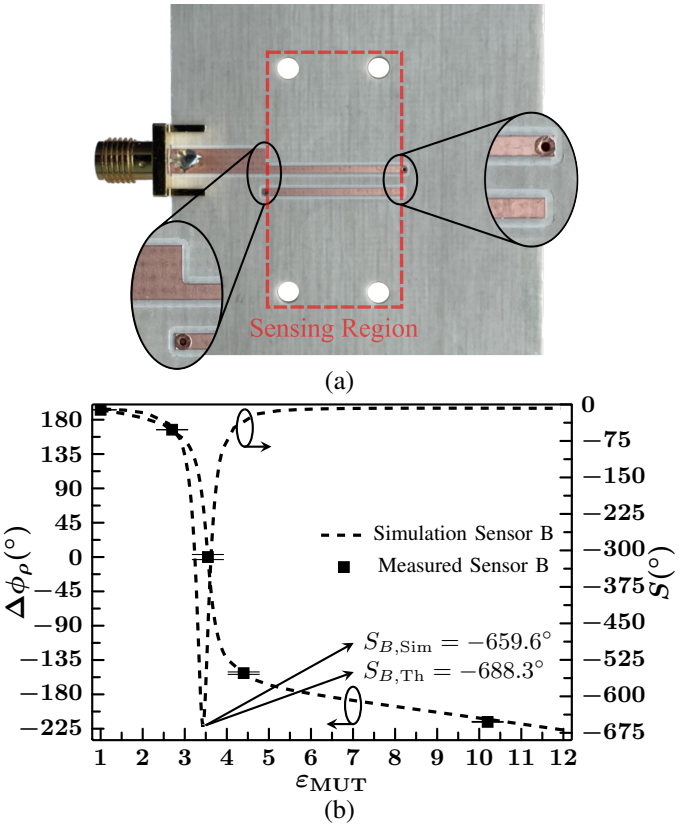

Fig. 6. Photograph of the fabricated sensor B with $\varepsilon_{\mathrm{REF}} = \varepsilon_r$ (a) and phase of the reflection coefficient at f_0 by varying the dielectric constant of the MUT and sensitivity (b). The sensing region is indicated with a dashed rectangle. Dimensions (in mm) are: $W = 1$, $g = 2$ and $l = 18.54$. The dimensions of the 50-Ω access lines (in mm) are: $W_0 = 3.33$, $l_0 = 12.8$.

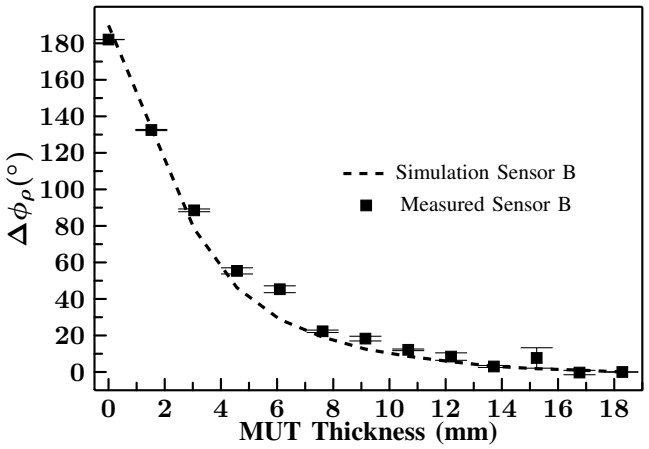

Fig. 7. Variation of the phase of the reflection coefficient for Sensor B with $\varepsilon_{\mathrm{REF}} = \varepsilon_r$ as a function of the sample thickness for a sample with dielectric constant of $\varepsilon_{\mathrm{MUT}} = \varepsilon_{\mathrm{REF}} = \varepsilon_r = 3.55$.

reach the boundaries of the MUT.

C. Sensor type B with weak coupling and $\varepsilon_{\mathrm{REF}} = 1$ (air)

The last prototype is also a type B sensor with weak coupling, but the REF material is air in this case ($\varepsilon_{\mathrm{REF}} = 1$). Let us designate this sensor as B', in order to distinguish it from the one of the previous subsection (sensor B). The geometry of the device [see Fig. 8(a)], provides even- and odd-mode characteristic impedances of $Z_{\mathrm{ev}} = 111.6\ \Omega$ and $Z_{\mathrm{od}} = 76.4\ \Omega$, respectively, achieving a coupling coefficient of $C = 0.19$. The simulated phase of the reflection coefficient, $\Delta\phi_\rho$, at f_0 as a function of the dielectric constant of the MUT is shown in Fig. 8(b). The thickness of the MUT has also been set to 18.3 mm, and the input dynamic range is also identical the one of the previous sensors. The sensitivity inferred from the simulated phase points is also included in Fig. 8(b). The value of the sensitivity for $\varepsilon_{\mathrm{MUT}} = \varepsilon_{\mathrm{REF}} = 1$ has been found to be $-736.0°$, i.e., in reasonable good agreement with the prediction of the theory, despite the fact that the REF material is air, with dielectric constant ($\varepsilon_{\mathrm{REF}} = 1$) significantly different to the one of the substrate ($\varepsilon_r = 3.55$).

Due to the lack of available MUT materials exhibiting a dielectric constant close to the one of air in our laboratory, validation of the capacity of the sensors to discriminate very small variations in the dielectric constant of the MUT in the vicinity of $\varepsilon_{\mathrm{REF}} = 1$ has been carried out by a different approach for this prototype sensor. In particular, we have considered a variable distance between the sensor and a stack of uncladded *Rogers RO4003C* substrates with a total thickness of 18.3 mm and dielectric constant 3.55, identical to the dielectric constant of the substrate. When the sample is sufficiently separated from the sensor, it is equivalent to consider a bare sensor (i.e., with $\varepsilon_{\mathrm{MUT}} = \varepsilon_{\mathrm{REF}} = 1$). However, as the sample progressively approaches the sensor, the equivalent dielectric constant of the MUT progressively increases, and it takes the maximum value when the dielectric sample is in contact with the sensor. The distance between the sensor and the dielectric (movable) slab has been achieved by means of the *Thorlabs MVS010/M - 25 mm Travel Vertical Translation Stage*, available in our laboratory. Note that, in this experiment, a multilayer structure composed of the air gap and the stack of uncladded substrates is considered. However, the aim of this experiment has been to detect small air gaps between the solid sample and the sensitive region of the sensor, rather than to characterize multilayer structures (see, e.g., [64], for that purpose)

The simulated and measured phases of the reflection coefficient as a function of the distance between the sensor and the movable sample are depicted in Fig. 8(c), and the agreement is very good. The quasi-saturation effect for high distances can be perfectly appreciated. For low separations between the sensor and the movable sample, the variation of the phase of the reflection coefficient with such separation is very significant, a consequence of the high sensitivity of such sensor.

V. Effects of Losses

In the analysis of Section III, the effects of conductor losses, as well as dielectric losses in both the MUT and the substrate material, have not been taken into account. This is reasonable provided the considered substrate is a commercial low-loss microwave substrate, and the MUT samples exhibit low losses (these conditions are fulfilled in the experimental validation of the previous section). However, it is necessary to determine

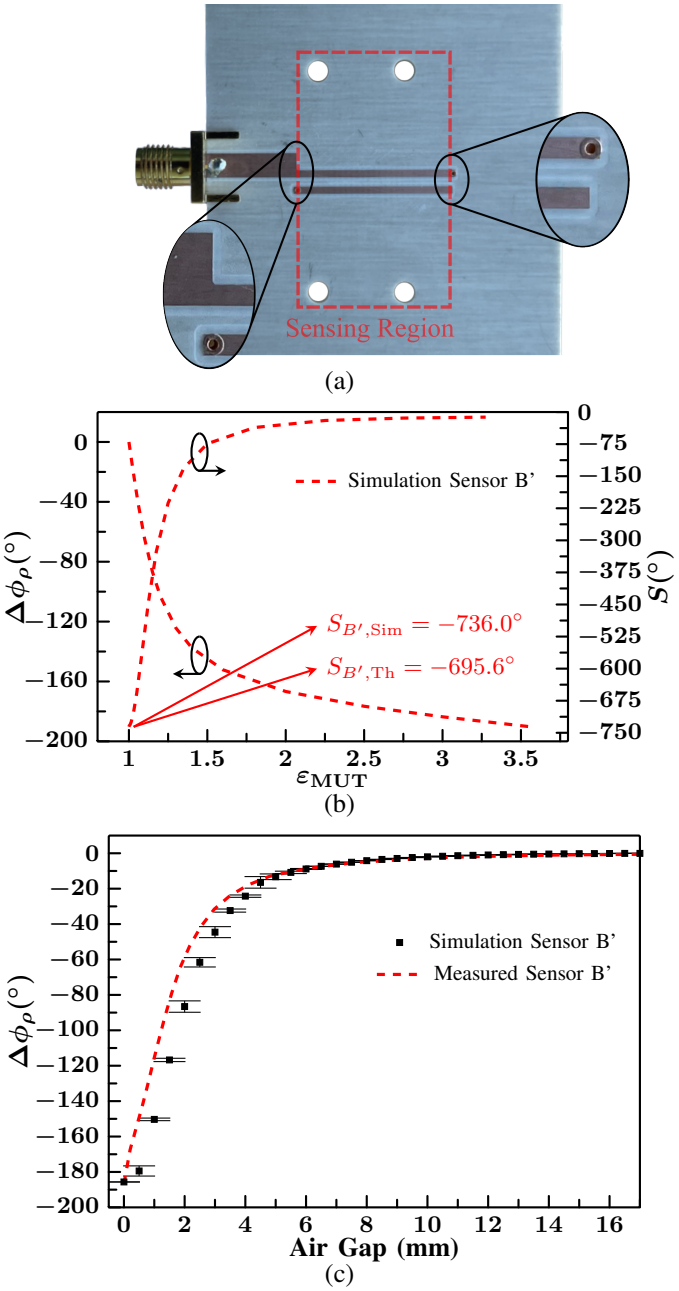

Fig. 8. Photograph of the fabricated sensor B' with $\varepsilon_{\mathrm{REF}} = 1$ (a), phase of the reflection coefficient at f_0 by varying the dielectric constant of the MUT and sensitivity (b), and phase of the reflection coefficient (at f_0) as a function of the distance between the sensor and the movable sample (c). The sensing region is indicated with a dashed rectangle. Dimensions (in mm) are: $W = 1$, $g = 1.25$ and $l = 21.84$. The dimensions of the 50-Ω access lines (in mm) are: $W_0 = 3.33$, $l_0 = 12.8$.

the limit of validity of the low-loss approximation, the main objective of this section. For this purpose, the effects of losses in the sensing structures are included by considering that the real part of the complex propagation constant, i.e., the attenuation constant, α, is not negligible.

Let us proceed by considering the weak coupling approximation with the presence of losses, and let us assume that, under this approximation, it is reasonable to consider that the complex propagation constant is identical for both modes (i.e., $\gamma_{\mathrm{ev}} \equiv \alpha_{\mathrm{ev}} + j\beta_{\mathrm{ev}} = \gamma_{\mathrm{od}} \equiv \alpha_{\mathrm{od}} + j\beta_{\mathrm{od}} = \gamma \equiv \alpha + j\beta$, where α and β are the attenuation and phase constants, respectively). If l is the length of the coupled lines, the elements of the impedance matrix with the presence of losses, and under the weak coupling approximation, are found to be

$$Z_{11} = Z_{22} = Z_{33} = Z_{44} = \frac{1}{2}\{Z_{\mathrm{ev}} + Z_{\mathrm{od}}\}\coth\gamma l \quad (25a)$$

$$Z_{12} = Z_{21} = Z_{34} = Z_{43} = \frac{1}{2}\{Z_{\mathrm{ev}} - Z_{\mathrm{od}}\}\coth\gamma l \quad (25b)$$

$$Z_{13} = Z_{31} = Z_{24} = Z_{42} = \frac{1}{2}\{Z_{\mathrm{ev}} - Z_{\mathrm{od}}\}\frac{1}{\sinh\gamma l} \quad (25c)$$

$$Z_{14} = Z_{41} = Z_{23} = Z_{32} = \frac{1}{2}\{Z_{\mathrm{ev}} + Z_{\mathrm{od}}\}\frac{1}{\sinh\gamma l} \quad (25d)$$

From these elements, the input impedance for each sensor type (A and B) can be obtained, and, from it, the phase of the reflection coefficient, the output variable, can be inferred.

Without loss of generality, let us focus the analysis specifically on sensor A. Using (2), the input impedance by considering losses can be expressed as

$$Z_{\mathrm{in},A} = \frac{(Z_{\mathrm{ev}} + Z_{\mathrm{od}})^2\cosh^2\gamma l - (Z_{\mathrm{ev}} - Z_{\mathrm{od}})^2}{2(Z_{\mathrm{ev}} + Z_{\mathrm{od}})\cosh\gamma l\sinh\gamma l} \quad (26)$$

After some straightforward mathematical calculation, the input impedance can be expressed as

$$Z_{\mathrm{in},A} = \frac{(Z_{\mathrm{ev}}+Z_{\mathrm{od}})^2(\cos 2\beta l\cosh 2\alpha l + j\sin 2\beta l\sinh 2\alpha l) - Z_{\mathrm{ev}}^2 - Z_{\mathrm{od}}^2 + 6Z_{\mathrm{ev}}Z_{od}}{2(Z_{\mathrm{ev}}+Z_{\mathrm{od}})(\cos 2\beta l\sinh 2\alpha l + j\sin 2\beta l\cosh 2\alpha l)} \quad (27)$$

If losses are small, $\sinh 2\alpha l \approx 2\alpha l$ and $\cosh 2\alpha l \approx 1$ (actually, $\cosh 2\alpha l \approx 1 + 2\alpha^2 l^2$, but the quadratic term can be neglected, provided $\alpha l \to 0$). Thus, the input impedance can be approximated by

$$Z_{\mathrm{in},A} = \frac{(Z_{\mathrm{ev}}+Z_{\mathrm{od}})^2\cos^2\beta l - (Z_{\mathrm{ev}}-Z_{\mathrm{od}})^2 + 2j\alpha l(Z_{\mathrm{ev}}+Z_{\mathrm{od}})^2\sin\beta l\cos\beta l}{(Z_{\mathrm{ev}}+Z_{\mathrm{od}})[2\alpha l(2\cos^2\beta l - 1) + 2j\sin\beta l\cos\beta l]} \quad (28)$$

It is apparent from (27), or (28), that in the limit when $\alpha l = 0$, the input impedance is identical to the one given by (6), since $\phi = \beta l$, as expected.

Once the input impedance is known, the reflection coefficient under the low-loss (and weak coupling) approximation can be calculated by means of (12). Note, however, that due to the presence of losses, the numerator and the denominator of the reflection coefficient are no longer conjugate numbers, and the phase cannot be directly inferred by means of (13). To obtain the phase of the reflection coefficient, the phase of the denominator needs to be subtracted from the phase of the numerator. Applying this procedure, and after some cumbersome calculation, the phase of the reflection coefficient can be expressed as

$$\phi_{\rho,A} = \arctan\left(-\frac{\chi_{\mathrm{in},A}}{Z_0}\frac{1-F_1}{1-F_2}\right) + \arctan\left(-\frac{\chi_{\mathrm{in},A}}{Z_0}\frac{1+F_1}{1+F_2}\right) \quad (29)$$

where $\chi_{\mathrm{in},A}$ is the input reactance when losses are absent, and F_1 and F_1 are dimensionless factors proportional to the attenuation constant, given by

$$F_1 = \frac{2\alpha l Z_0(Z_{\mathrm{ev}} + Z_{\mathrm{od}})(2\cos^2\beta l - 1)}{(Z_{\mathrm{ev}} + Z_{\mathrm{od}})^2\cos^2\beta l - (Z_{\mathrm{ev}} - Z_{\mathrm{od}})^2} \quad (30a)$$

$$F_2 = \frac{\alpha l(Z_{\mathrm{ev}} + Z_{\mathrm{od}})}{Z_0} \quad (30b)$$

It is obvious that for low losses, both F_1 and F_2 are negligible, and the phase of the reflection coefficient coincides with the one of the lossless case, given by (13). However, to quantify the validity of the low-loss approximation, let us force (30a) and (30b) to satisfy $F_1 \ll 1$ and $F_2 \ll 1$, sufficient conditions for obtaining a phase of the reflection coefficient insensitive to the effects of losses. From (30a), the following condition results

$$\frac{\alpha l}{C} \ll \frac{Z_{\rm ev} - Z_{\rm od}}{Z_0} \frac{\left(\frac{\cos^2 \beta l}{C^2} - 1\right)}{2(2\cos^2 \beta l - 1)} \tag{31a}$$

whereas from (30b), the inequality that should be satisfied is

$$\frac{\alpha l}{C} \ll \frac{Z_0}{Z_{\rm ev} - Z_{\rm od}} \tag{31b}$$

In (31), the coupling factor, C, defined in (7), is used. In principle, the more restrictive condition among (31a) and (31b) should be the one considered for the validity of the low-loss approximation. However, (31a) depends on the phase of the coupled lines, and there are values of the phase, i.e., those given by (7), that null the right-hand side member. Obviously, for phases close to these values, (30a) cannot be satisfied, and F_1 takes large values. Nevertheless, the arguments of the $\arctan$ in (29) are finite, because $\chi_{{\rm in},A}$ nulls for these phase values. The result is that the arguments of the $\arctan$ in (29) are not strictly null, but are small. Let us consider the worst case, which corresponds to the phases satisfying (7). For such phases, the reactance for the lossless case is null. Therefore, in order to find the limiting values of αl for these phases, it is necessary to force the magnitude of the arguments in the $\arctan$ in (29) to be significantly smaller than 1. This gives

$$\frac{\alpha l}{C} \ll \frac{Z_0\sqrt{1-C^2}}{Z_0(1-2C^2)+C\sqrt{1-C^2}(Z_{\rm ev}+Z_{\rm od})} \approx \frac{Z_0}{Z_0+Z_{\rm ev}-Z_{\rm od}} \tag{32}$$

Note that (32) is more restrictive than (31b).

Other singular phases are those that open the lossless input reactance, i.e., $\phi = \beta l = 90^\circ$ and odd multiples. For these phases, (31a) gives

$$\frac{\alpha l}{C} \ll \frac{Z_{\rm ev} - Z_{\rm od}}{2Z_0} \tag{33}$$

which is even more restrictive than (32), especially for weakly coupled lines. Therefore, (33) is the condition that should be satisfied in order to ensure that losses do not alter the phase of the reflection coefficient, as compared to the one of the lossless case. Other singular phases are those that null the numerator in (30a), and those providing $\cos^2 \beta l = 1$. In the former case, F_1 is null. In the second case, the condition that results from (31a) is much less restrictive than (33).

Let us now estimate if condition (33) is reasonably fulfilled by considering low-loss samples, as those considered in the experimental validation of the proposed sensors. Exact calculation of the attenuation constant is not simple, as far as the considered coupled lines are open (though covered by the MUT). Such exact calculation is indeed out of the scope of this paper. Nevertheless, let us assume that the attenuation constant is similar to the one of an isolated line with characteristic impedance Z. For low losses, such attenuation constant is given by [62]

$$\alpha l = \frac{1}{2}\left(\frac{R}{Z} + GZ\right) \tag{34}$$

where R and G are the resistance and conductance of the line, respectively. The resistance R depends on the resistivity of the metallic layer (typically copper in low-loss commercial microwave substrates), on the transverse geometry and length of the line, as well as on the operating frequency (due to the skin effect). The conductance of the line is determined by the loss tangent of the substrate, $\tan\delta$, by the loss tangent of the MUT, $\tan\delta_{\rm MUT}$, and by the length and transverse geometry of the line. In closed lines surrounded by a uniform material with well-known loss tangent (the one of the substrate), the conductance can be expressed in terms of the capacitance of the line, C_l, and operating angular frequency, ω, according to [62]

$$G = C_l \omega \tan\delta \tag{35}$$

In our case, where a MUT is on top of the sensor line structure, uniformity is not fulfilled unless the MUT is identical to the substrate material. Nevertheless, the conductance of the line can be formally expressed as (35), by replacing the loss tangent of the substrate, $\tan\delta$, with an equivalent loss tangent, $\tan\delta_{\rm eq}$, that, obviously, depends on the line geometry, and should be related to the loss tangent of the substrate and MUT.

Typically, line losses are dominated by dielectric losses. Therefore, the contribution of conductor losses are neglected in the present analysis, and the attenuation constant can be simplified to

$$\alpha l = \frac{ZC_l\omega}{2}\tan\delta_{\rm eq} = \frac{\omega\sqrt{L_lC_l}}{2}\tan\delta_{\rm eq} = \frac{\phi}{2}\tan\delta_{\rm eq} \tag{36}$$

where L_l is the inductance of the line. Introduction of (36) in (33) gives the following condition, representing an inferior limit to the coupling factor,

$$C^2 \gg \frac{Z_0}{Z_{\rm ev} + Z_{\rm od}}\phi\tan\delta_{\rm eq} \tag{37}$$

Thus, weak coupling favors sensitivity enhancement, but, in order to implement a sensor where the phase of the reflection coefficient, the output variable, is insensitive to the effects of the loss tangent of the MUT (thereby circumventing this cross-sensitivity), the coupling factor must satisfy (37). Note, however, that for small perturbations, the phase is roughly $\phi \approx \pi/2$. For even and odd mode impedances comparable to the reference impedance of the ports, the impedance quotient in the right-hand side member of (37) is of the order of 0.5. Using these values, and considering low-loss substrates and MUTs, providing equivalent loss tangents of the order of 0.001-0.005, it follows that the coupling factor must satisfy $C^2 \gg 0.004$ (corresponding to the upper equivalent loss tangent in the indicated interval). According to this estimation, by designing the coupled lines of a generic sensor type A with a coupling factor of the order of, e.g., $C = 0.2$, the above condition is satisfied. Moreover, a sensitivity enhancement of $1/C^2 = 25$, as compared to the one of the sensor based on an isolated line [see (16) and (22)], is achieved with such coupling factor.

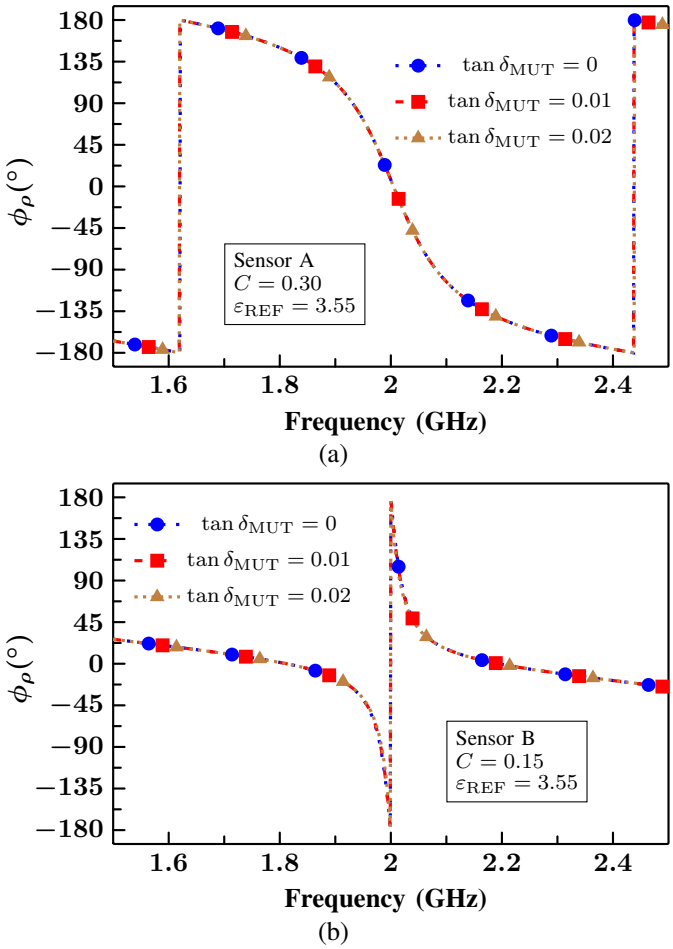

Fig. 9. Simulated phase of the reflection coefficient as a function of frequency for Sensor A, when it is covered with the REF material, with dielectric constant $\varepsilon_{\rm REF} = 3.55$, but different loss tangents (a). Simulated phase of the reflection coefficient as a function of frequency for Sensor B, when is covered with REF material, with $\varepsilon_{\rm REF} = 3.55$, but different loss tangents (b). Note that the coupling factor for Sensor A is $C = 0.30$, and $C = 0.15$ for Sensor B.

In order to validate the previous discussion in regard to the effects of losses, we have carried out electromagnetic simulations of Sensors of A and B covered with the REF material, but considering that it exhibits different loss tangents. We have obtained the phase of the reflection coefficient as a function of frequency (equivalent to modify the phase of the coupled lines), rather than obtaining the dependence with the dielectric constant of the MUT. The results, depicted in Fig. 9, reveal that the effects of losses are irrelevant in the considered range of variation of the loss tangent of the MUT. Therefore, the previous loss analysis is validated. Moreover, it is demonstrated that for low-loss materials, the phase of the reflection coefficient does not exhibit cross-sensitivity with the loss tangent of the MUT, an important aspect to accurately determine the dielectric constant of the MUT, the input variable.

For the accurate measurement of the loss tangent of low-loss materials, resonant cavities are preferred [65]–[68] and are commercially available. The proposed sensor is suitable for the accurate measurement of the dielectric constant of low-loss materials, as indicated. However, it is also useful for measuring other variables related to the dielectric constant of the MUT. For example, the proposed sensors can be useful to detect tiny defects in samples, as far as such defects perturb the equivalent dielectric constant of the samples. Another application that can be envisaged is the accurate determination of the composition of liquid mixtures, since the relative concentration of the different components has direct influence on the complex dielectric constant of the mixture. It has also been shown in Section IV-C that the phase of the reflection coefficient (the output variable) of the sensor considered in that section is very sensitive to the separation (or vertical distance) between the sensor and a certain dielectric sample present (contactless) on top of it. This means that, besides dielectric characterization (the canonical application of permittivity sensors), the proposed highly sensitive sensors can alternatively be used as accurate position sensors. Nevertheless, the present paper has been mainly focused on demonstrating the potential for sensitivity enhancement of the proposed coupled-line based sensors, rather than implementing specific sensors devoted to the indicated potential applications.

VI. Comparison with other phase-variation sensors

The main relevant aspect of the reflective-mode phase-variation sensors based on coupled lines reported in this work is the highly achievable sensitivity. As it has been demonstrated, such high sensitivities are related to the significant phase slope present between the two split resonances when the lines are weakly coupled. In the sensor of Section IV-B, the maximum sensitivity has been found to be $|S| = 659.6°$, whereas a value of $|S| = 736.0°$ has been obtained in the sensor reported in Section IV-C. Such high (unprecedented) sensitivities have been obtained without the need of cascading additional quarter-wavelength high/low impedance line sections, contrary to the reflective-mode phase-variation sensors reported in [6]–[8], where the sensing region is either an open-ended high-impedance quarter-wavelength line section (equivalent to a grounded series resonator) or an open-ended low-impedance half-wavelength line section (equivalent to a grounded parallel resonator). The best reported sensitivity in these sensors based on open-ended quarter- or half-wavelength resonators is 528.7° [6], clearly below the values given above, achieved in the present work. Moreover, such high sensitivity achieved in the sensor reported in [6], has been obtained by cascading two quarter-wavelength line sections (one section with high characteristic impedance and the other one with low characteristic impedance) to the main sensing line, which represents a penalty in terms of the overall sensor size.

A comparison of different phase-variation sensors is given in Table I, where the operating mode (transmission, TX, or reflection, RX), the maximum sensitivity, the size of the overall sensor (excluding the access lines), the size of the sensing region, both expressed in terms of the squared guided wavelength, as well as the figure of merit (FoM), defined as the ratio between the maximum sensitivity and size of the sensing region, are included. Since sensitivity enhancement is achieved

TABLE I
COMPARISON OF VARIOUS PHASE-VARIATION PERMITTIVITY SENSORS

Ref.	Mode	Sensing size* (λ^2)	Overall size (λ^2)	Max. Sensitivity	$\Delta\varepsilon_{\mathrm{MUT,HM}}$	FoM ($^\circ/\lambda^2$)
[1]	TX	—	—	600 dB	—	—
[2]	TX	—	—	54.8°	—	—
[3]	TX	12.90	12.90	415.6°	—	32.2
[4]	TX	0.075	0.075	25.3 dB	—	—
[5]	TX	0.020	0.40	17.6 dB	—	—
[6]	RX	0.025	0.131	528.7°	0.4	21148
[7]	RX	0.100	0.297	45.5°	3	455
[8]	RX	0.065	0.126	101.3°	2.4	1558
[9]	TX	0.030	0.090	7.7°	—	257
[10]	TX	0.040	0.054	20.0°	10	500
[11]	TX	0.038	0.053	12.3°	7	332
[12]	RX	0.015	0.073	83.35°	1.5	5643
[13]	RX	0.018	0.076	66.5°	3.75	3643
Sens. B	**RX**	**0.070**	**0.070**	**659.6°**	**0.33**	**9401**
Sens. B'	**RX**	**0.058**	**0.058**	**736.0°**	**0.15**	**12690**

* This size corresponds to the sensing region, not to the size of the whole sensing structure, referred to as overall size and indicated in the adjacent column to the right.

at the expense of linearity degradation (i.e., the sensitivity is not constant), it is convenient to include in the table the range of dielectric constants of the MUT where the sensitivity is above half the maximum value. Such range of dielectric constants is designated as $\Delta\varepsilon_{\mathrm{MUT,HM}}$ in the table. According to Table I, the proposed sensors exhibit the best sensitivity, with very small sensor size, which coincides with the size of the sensing region, since no further additional elements are used to boost up the sensitivity (as in the sensors of [6]–[8]), or to transform the phase information to magnitude information (e.g., as in the sensor reported in [1], [4], [5]).

As it can be seen in Table I, the FoM is better in the sensor reported in [6], mainly because the sensing region in those sensors consists merely of an open-ended line section. However, it should be mentioned that the unprecedented maximum sensitivity of the coupled-line based sensors of this work has been obtained without the need of introducing further elements to the sensing region (thereby achieving a very competitive overall sensor size). Moreover, the sensitivity can be further enhanced by merely reducing the coupling coefficient, C, of the coupled lines, i.e., by simply increasing the distance between the lines (this does not represent a significant increase in the sensor size).

Note that in the table, there are three sensors where the sensitivity is given in dB. The reason is that in such sensors, the phase is transformed to magnitude information. In [5], the device is a differential sensor based on meander lines, and phase to magnitude conversion is achieved by means of a pair of rat-race couplers. The sensitivity in these sensors is reasonably good, and sensor design is simple, but the total sensor size is large due to the presence of the two rat-race couplers. In the sensors of [1], [4], both based on artificial lines, the sensitivity and the size of the sensing region is very competitive, but their robustness is limited, due to potential effects of detuning (this is particularly critical in the narrowband structures based on electroinductive-wave (EIW) transmission lines [4]).

In summary, the reflective-mode phase-variation coupled-line based sensors presented in this work exhibit a good combination of size (overall sensor and sensing region) and sensitivity. Indeed, to the best of the authors' knowledge, the sensitivities obtained in this work are the highest achieved sensitivities in phase-variation microwave sensors. Let us also mention that sensor design is simple, and the maximum sensitivity can be reasonably predicted under the weak coupling approximation, of interest since weak coupling is necessary to boost up the sensitivity.

VII. CONCLUSION

In conclusion, a new type of reflective-mode phase-variation permittivity sensors, based on coupled lines (the sensitive region), has been reported in this paper. It has been demonstrated that by properly terminating three of the four ports of the pair of coupled lines, the resulting one-port structure is highly sensitive to variations in the dielectric constant of the MUT, provided the lines are weakly coupled. The sensing regions of the two considered sensor types (designated as A and B in this paper) behave as a pair of weakly coupled quarter-wavelength resonators. Consequently, the phase of the reflection coefficient exhibits a variation of 360° between the two split resonance frequencies, necessarily very closely spaced by virtue of the weak coupling. Thus, weak inter-resonator coupling is the principle for sensitivity enhancement in the reported coupled-line based sensors, as it has been analytically demonstrated and experimentally validated. Indeed, it has been shown that the maximum sensitivity is inversely proportional to the square of the coupling coefficient of the pair of coupled lines. Maximum sensitivities of 659.6° and 736° have been achieved in two of the designed and fabricated prototype sensors, i.e., unprecedented values in phase-variation microwave sensors. The proposed strategy for sensitivity optimization merely utilizes a pair of coupled lines, contrary to other similar reflective-mode sensors based on quarter-wavelength, or half-wavelength, open-ended sensing lines, where sensitivity enhancement is achieved by cascading high/low impedance quarter-wavelength transmission line sections. The resulting figures of merit (FoM) in the reported sensors, defined as the ratio between the maximum sensitivity and the area of the sensing region expressed in terms of the squared wavelength, are as high as $9401^\circ/\lambda^2$ and $12690^\circ/\lambda^2$. These values are competitive and have been achieved without the need of adding further stages to the sensing region. Therefore, the potential of the reported coupled line structures to implement highly sensitive permittivity sensors with a small sensing region and with a limited size of the whole sensor structure, has been demonstrated. The reported sensors are of special interest in applications where high sensitivity in the detection of the dielectric constant of the MUT or related variables is needed, including, defect detection in samples (e.g., corrosion, or structural health monitoring), measurement of liquid composition or contaminants in liquids (microfluidics), highly sensitive position or proximity sensors, biosensing, etc.

REFERENCES

[1] C. Damm, M. Schüßler, M. Puentes, H. Maune, M. Maasch, and R. Jakoby, "Artificial transmission lines for high sensitive microwave sensors," in *2009 IEEE SENSORS*, Oct. 2009, pp. 755–758.

[2] F. J. Ferrández-Pastor, J. M. García-Chamizo, and M. Nieto-Hidalgo, "Electromagnetic Differential Measuring Method: Application in Microstrip Sensors Developing," *Sensors*, vol. 17, no. 7, p. 1650, Jul. 2017.

[3] J. Muñoz-Enano, P. Vélez, M. Gil Barba, and F. Martín, "An Analytical Method to Implement High-Sensitivity Transmission Line Differential Sensors for Dielectric Constant Measurements," *IEEE Sensors J.*, vol. 20, no. 1, pp. 178–184, Jan. 2020.

[4] M. Gil, P. Vélez, F. Aznar-Ballesta, J. Muñoz-Enano, and F. Martín, "Differential Sensor Based on Electroinductive Wave Transmission Lines for Dielectric Constant Measurements and Defect Detection," *IEEE Trans. Antennas Propag.*, vol. 68, no. 3, pp. 1876–1886, Mar. 2020.

[5] J. Muñoz-Enano, P. Vélez, M. Gil Barba, J. Mata-Contreras, and F. Martín, "Differential-Mode to Common-Mode Conversion Detector Based on Rat-Race Hybrid Couplers: Analysis and Application to Differential Sensors and Comparators," *IEEE Trans. Microw. Theory Tech.*, vol. 68, no. 4, pp. 1312–1325, Apr. 2020.

[6] J. Muñoz-Enano, P. Vélez, L. Su, M. Gil, P. Casacuberta, and F. Martín, "On the Sensitivity of Reflective-Mode Phase-Variation Sensors Based on Open-Ended Stepped-Impedance Transmission Lines: Theoretical Analysis and Experimental Validation," *IEEE Trans. Microw. Theory Tech.*, vol. 69, no. 1, pp. 308–324, Jan. 2021.

[7] L. Su, J. Muñoz-Enano, P. Velez, P. Casacuberta, M. Gil, and F. Martín, "Highly Sensitive Phase Variation Sensors Based on Step-Impedance Coplanar Waveguide (CPW) Transmission Lines," *IEEE Sensors J.*, vol. 21, no. 3, pp. 2864–2872, Feb. 2021.

[8] P. Casacuberta, J. Muñoz-Enano, P. Vélez, L. Su, M. Gil, and F. Martín, "Highly Sensitive Reflective-Mode Defect Detectors and Dielectric Constant Sensors Based on Open-Ended Stepped-Impedance Transmission Lines," *Sensors*, vol. 20, no. 21, p. 6236, Jan. 2020.

[9] J. Coromina, J. Muñoz-Enano, P. Vélez, A. Ebrahimi, J. Scott, K. Ghorbani, and F. Martín, "Capacitively-Loaded Slow-Wave Transmission Lines for Sensitivity Improvement in Phase-Variation Permittivity Sensors," in *2020 50th European Microwave Conference (EuMC)*, Jan. 2021, pp. 491–494.

[10] A. Ebrahimi, J. Coromina, J. Muñoz-Enano, P. Vélez, J. Scott, K. Ghorbani, and F. Martín, "Highly Sensitive Phase-Variation Dielectric Constant Sensor Based on a Capacitively-Loaded Slow-Wave Transmission Line," *IEEE Trans. Circuits Syst. Regul. Pap.*, vol. 68, no. 7, pp. 2787–2799, Jul. 2021.

[11] L. Su, J. Muñoz-Enano, P. Vélez, P. Casacuberta, M. Gil, and F. Martín, "Phase-Variation Microwave Sensor for Permittivity Measurements Based on a High-Impedance Half-Wavelength Transmission Line," *IEEE Sensors J.*, vol. 21, no. 9, pp. 10 647–10 656, May 2021.

[12] L. Su, J. Muñoz-Enano, P. Vélez, M. Gil-Barba, P. Casacuberta, and F. Martín, "Highly Sensitive Reflective-Mode Phase-Variation Permittivity Sensor Based on a Coplanar Waveguide Terminated With an Open Complementary Split Ring Resonator (OCSRR)," *IEEE Access*, vol. 9, pp. 27 928–27 944, 2021.

[13] P. Casacuberta, P. Vélez, J. Muñoz-Enano, L. Su, M. G. Barba, A. Ebrahimi, and F. Martín, "Circuit Analysis of a Coplanar Waveguide (CPW) Terminated With a Step-Impedance Resonator (SIR) for Highly Sensitive One-Port Permittivity Sensing," *IEEE Access*, vol. 10, pp. 62 597–62 612, 2022.

[14] A. K. Jha, A. Lamecki, M. Mrozowski, and M. Bozzi, "A Highly Sensitive Planar Microwave Sensor for Detecting Direction and Angle of Rotation," *IEEE Trans. Microw. Theory Tech.*, vol. 68, no. 4, pp. 1598–1609, Apr. 2020.

[15] A. K. Horestani, Z. Shaterian, and F. Martín, "Rotation Sensor Based on the Cross-Polarized Excitation of Split Ring Resonators (SRRs)," *IEEE Sensors J.*, vol. 20, no. 17, pp. 9706–9714, Sep. 2020.

[16] J. Muñoz-Enano, P. Vélez, L. Su, M. Gil-Barba, and F. Martín, "A Reflective-Mode Phase-Variation Displacement Sensor," *IEEE Access*, vol. 8, pp. 189 565–189 575, 2020.

[17] M. Puentes, C. Weiß, M. Schüßler, and R. Jakoby, "Sensor array based on split ring resonators for analysis of organic tissues," in *2011 IEEE MTT-S International Microwave Symposium*, Jun. 2011, pp. 1–4.

[18] A. Ebrahimi, W. Withayachumnankul, S. Al-Sarawi, and D. Abbott, "High-Sensitivity Metamaterial-Inspired Sensor for Microfluidic Dielectric Characterization," *IEEE Sensors J.*, vol. 14, no. 5, pp. 1345–1351, May 2014.

[19] M. Schüßler, C. Mandel, M. Puentes, and R. Jakoby, "Metamaterial Inspired Microwave Sensors," *IEEE Microw. Mag.*, vol. 13, no. 2, pp. 57–68, Mar. 2012.

[20] M. S. Boybay and O. M. Ramahi, "Material Characterization Using Complementary Split-Ring Resonators," *IEEE Trans. Instrum. Meas.*, vol. 61, no. 11, pp. 3039–3046, Nov. 2012.

[21] C.-S. Lee and C.-L. Yang, "Complementary Split-Ring Resonators for Measuring Dielectric Constants and Loss Tangents," *IEEE Microw. Wirel. Compon. Lett.*, vol. 24, no. 8, pp. 563–565, Aug. 2014.

[22] C.-L. Yang, C.-S. Lee, K.-W. Chen, and K.-Z. Chen, "Noncontact Measurement of Complex Permittivity and Thickness by Using Planar Resonators," *IEEE Trans. Microw. Theory Tech.*, vol. 64, no. 1, pp. 247–257, Jan. 2016.

[23] L. Su, J. Mata-Contreras, P. Vélez, and F. Martín, "Estimation of the complex permittivity of liquids by means of complementary split ring resonator (CSRR) loaded transmission lines," in *2017 IEEE MTT-S International Microwave Workshop Series on Advanced Materials and Processes for RF and THz Applications (IMWS-AMP)*, Sep. 2017, pp. 1–3.

[24] L. Su, J. Mata-Contreras, P. Vélez, A. Fernández-Prieto, and F. Martín, "Analytical Method to Estimate the Complex Permittivity of Oil Samples," *Sensors*, vol. 18, no. 4, p. 984, Apr. 2018.

[25] A. K. Jha, N. Delmonte, A. Lamecki, M. Mrozowski, and M. Bozzi, "Design of Microwave-Based Angular Displacement Sensor," *IEEE Microw. Wirel. Compon. Lett.*, vol. 29, no. 4, pp. 306–308, Apr. 2019.

[26] A. Horestani, J. Naqui, D. Abbott, C. Fumeaux, and F. Martín, "Two-dimensional displacement and alignment sensor based on reflection coefficients of open microstrip lines loaded with split ring resonators," *Electron. Lett.*, vol. 50, no. 8, pp. 620–622, 2014.

[27] J. Naqui, C. Damm, A. Wiens, R. Jakoby, L. Su, and F. Martín, "Transmission lines loaded with pairs of magnetically coupled stepped impedance resonators (SIRs): Modeling and application to microwave sensors," in *2014 IEEE MTT-S International Microwave Symposium (IMS2014)*, Jun. 2014, pp. 1–4.

[28] L. Su, J. Naqui, J. Mata-Contreras, and F. Martín, "Modeling Metamaterial Transmission Lines Loaded With Pairs of Coupled Split-Ring Resonators," *IEEE Antennas Wirel. Propag. Lett.*, vol. 14, pp. 68–71, 2015.

[29] ——, "Modeling and Applications of Metamaterial Transmission Lines Loaded With Pairs of Coupled Complementary Split-Ring Resonators (CSRRs)," *IEEE Antennas Wirel. Propag. Lett.*, vol. 15, pp. 154–157, 2016.

[30] J. Naqui, C. Damm, A. Wiens, R. Jakoby, L. Su, J. Mata-Contreras, and F. Martín, "Transmission Lines Loaded With Pairs of Stepped Impedance Resonators: Modeling and Application to Differential Permittivity Measurements," *IEEE Trans. Microw. Theory Tech.*, vol. 64, no. 11, pp. 3864–3877, Nov. 2016.

[31] L. Su, J. Mata-Contreras, P. Vélez, and F. Martín, "Splitter/Combiner Microstrip Sections Loaded With Pairs of Complementary Split Ring Resonators (CSRRs): Modeling and Optimization for Differential Sensing Applications," *IEEE Trans. Microw. Theory Tech.*, vol. 64, no. 12, pp. 4362–4370, Dec. 2016.

[32] P. Vélez, L. Su, K. Grenier, J. Mata-Contreras, D. Dubuc, and F. Martín, "Microwave Microfluidic Sensor Based on a Microstrip Splitter/Combiner Configuration and Split Ring Resonators (SRRs) for Dielectric Characterization of Liquids," *IEEE Sensors J.*, vol. 17, no. 20, pp. 6589–6598, Oct. 2017.

[33] J. Naqui, M. Durán-Sindreu, and F. Martín, "Novel Sensors Based on the Symmetry Properties of Split Ring Resonators (SRRs)," *Sensors*, vol. 11, no. 8, pp. 7545–7553, Aug. 2011.

[34] ——, "Alignment and Position Sensors Based on Split Ring Resonators," *Sensors*, vol. 12, no. 9, pp. 11 790–11 797, Sep. 2012.

[35] A. K. Horestani, C. Fumeaux, S. F. Al-Sarawi, and D. Abbott, "Displacement Sensor Based on Diamond-Shaped Tapered Split Ring Resonator," *IEEE Sensors J.*, vol. 13, no. 4, pp. 1153–1160, Apr. 2013.

[36] A. K. Horestani, D. Abbott, and C. Fumeaux, "Rotation Sensor Based on Horn-Shaped Split Ring Resonator," *IEEE Sensors J.*, vol. 13, no. 8, pp. 3014–3015, Aug. 2013.

[37] J. Naqui and F. Martín, "Transmission Lines Loaded With Bisymmetric Resonators and Their Application to Angular Displacement and Velocity Sensors," *IEEE Trans. Microw. Theory Tech.*, vol. 61, no. 12, pp. 4700–4713, Dec. 2013.

[38] ——, "Angular Displacement and Velocity Sensors Based on Electric-LC (ELC) Loaded Microstrip Lines," *IEEE Sensors J.*, vol. 14, no. 4, pp. 939–940, Apr. 2014.

[39] A. K. Horestani, J. Naqui, Z. Shaterian, D. Abbott, C. Fumeaux, and F. Martín, "Two-dimensional alignment and displacement sensor

based on movable broadside-coupled split ring resonators," *Sensors and Actuators A: Physical*, vol. 210, pp. 18–24, Apr. 2014.
[40] A. Ebrahimi, W. Withayachumnankul, S. F. Al-Sarawi, and D. Abbott, "Metamaterial-Inspired Rotation Sensor With Wide Dynamic Range," *IEEE Sensors J.*, vol. 14, no. 8, pp. 2609–2614, Aug. 2014.
[41] J. Naqui, J. Coromina, A. Karami-Horestani, C. Fumeaux, and F. Martín, "Angular Displacement and Velocity Sensors Based on Coplanar Waveguides (CPWs) Loaded with S-Shaped Split Ring Resonators (S-SRR)," *Sensors*, vol. 15, no. 5, pp. 9628–9650, May 2015.
[42] J. Mata-Contreras, C. Herrojo, and F. Martín, "Application of Split Ring Resonator (SRR) Loaded Transmission Lines to the Design of Angular Displacement and Velocity Sensors for Space Applications," *IEEE Trans. Microw. Theory Tech.*, vol. 65, no. 11, pp. 4450–4460, Nov. 2017.
[43] ——, "Detecting the Rotation Direction in Contactless Angular Velocity Sensors Implemented With Rotors Loaded With Multiple Chains of Resonators," *IEEE Sensors J.*, vol. 18, no. 17, pp. 7055–7065, Sep. 2018.
[44] G. Galindo-Romera, F. Javier Herraiz-Martínez, M. Gil, J. J. Martínez-Martínez, and D. Segovia-Vargas, "Submersible Printed Split-Ring Resonator-Based Sensor for Thin-Film Detection and Permittivity Characterization," *IEEE Sensors J.*, vol. 16, no. 10, pp. 3587–3596, May 2016.
[45] K. Grenier, D. Dubuc, P.-E. Poleni, M. Kumemura, H. Toshiyoshi, T. Fujii, and H. Fujita, "Integrated Broadband Microwave and Microfluidic Sensor Dedicated to Bioengineering," *IEEE Trans. Microw. Theory Tech.*, vol. 57, no. 12, pp. 3246–3253, Dec. 2009.
[46] T. Chretiennot, D. Dubuc, and K. Grenier, "A Microwave and Microfluidic Planar Resonator for Efficient and Accurate Complex Permittivity Characterization of Aqueous Solutions," *IEEE Trans. Microw. Theory Tech.*, vol. 61, no. 2, pp. 972–978, Feb. 2013.
[47] A. Salim, S.-H. Kim, J. Y. Park, and S. Lim, "Microfluidic Biosensor Based on Microwave Substrate-Integrated Waveguide Cavity Resonator," *J. Sens.*, vol. 2018, p. e1324145, Feb. 2018.
[48] M. H. Zarifi, H. Sadabadi, S. H. Hejazi, M. Daneshmand, and A. Sanati-Nezhad, "Noncontact and Nonintrusive Microwave-Microfluidic Flow Sensor for Energy and Biomedical Engineering," *Sci Rep*, vol. 8, no. 1, p. 139, Jan. 2018.
[49] P. Vélez, K. Grenier, J. Mata-Contreras, D. Dubuc, and F. Martín, "Highly-Sensitive Microwave Sensors Based on Open Complementary Split Ring Resonators (OCSRRs) for Dielectric Characterization and Solute Concentration Measurement in Liquids," *IEEE Access*, vol. 6, pp. 48 324–48 338, 2018.
[50] P. Vélez, J. Muñoz-Enano, K. Grenier, J. Mata-Contreras, D. Dubuc, and F. Martín, "Split Ring Resonator-Based Microwave Fluidic Sensors for Electrolyte Concentration Measurements," *IEEE Sensors J.*, vol. 19, no. 7, pp. 2562–2569, Apr. 2019.
[51] P. Vélez, J. Muñoz-Enano, M. Gil, J. Mata-Contreras, and F. Martín, "Differential Microfluidic Sensors Based on Dumbbell-Shaped Defect Ground Structures in Microstrip Technology: Analysis, Optimization, and Applications," *Sensors*, vol. 19, no. 14, p. 3189, Jan. 2019.
[52] J. Muñoz-Enano, P. Vélez, M. Gil, and F. Martín, "Microfluidic reflective-mode differential sensor based on open split ring resonators (OSRRs)," *Int. J. Microw. Wirel. Technol.*, vol. 12, no. 7, pp. 588–597, Sep. 2020.
[53] A. M. Albishi, M. K. E. Badawe, V. Nayyeri, and O. M. Ramahi, "Enhancing the Sensitivity of Dielectric Sensors With Multiple Coupled Complementary Split-Ring Resonators," *IEEE Trans. Microw. Theory Tech.*, vol. 68, no. 10, pp. 4340–4347, Oct. 2020.
[54] M. Abdolrazzaghi, M. Daneshmand, and A. K. Iyer, "Strongly Enhanced Sensitivity in Planar Microwave Sensors Based on Metamaterial Coupling," *IEEE Trans. Microw. Theory Tech.*, vol. 66, no. 4, pp. 1843–1855, Apr. 2018.
[55] C. G. Juan, B. Potelon, C. Quendo, E. Bronchalo, and J. M. Sabater-Navarro, "Highly-Sensitive Glucose Concentration Sensor Exploiting Inter-resonators Couplings," in *2019 49th European Microwave Conference (EuMC)*, Oct. 2019, pp. 662–665.
[56] Z. Xu, Y. Wang, and S. Fang, "Dielectric Characterization of Liquid Mixtures Using EIT-like Transmission Window," *IEEE Sensors J.*, vol. 21, no. 16, pp. 17 859–17 867, Aug. 2021.
[57] I. Piekarz, J. Sorocki, K. Wincza, and S. Gruszczynski, "Microwave Sensors for Dielectric Sample Measurement Based on Coupled-Line Section," *IEEE Trans. Microw. Theory Tech.*, vol. 65, no. 5, pp. 1615–1631, May 2017.
[58] J. Sorocki, I. Piekarz, K. Wincza, S. Gruszczynski, and J. Papapolymerou, "Broadband Microwave Microfluidic Coupled-Line Sensor With 3-D-Printed Channel for Industrial Applications," *IEEE Trans. Microw. Theory Tech.*, vol. 68, no. 7, pp. 2808–2822, Jul. 2020.
[59] I. Piekarz, J. Sorocki, K. Wincza, and S. Gruszczynski, "Coupled-Line Sensor With Marchand Balun as RF System for Dielectric Sample Detection," *IEEE Sensors J.*, vol. 16, no. 1, pp. 88–96, Jan. 2016.
[60] Z. R. Omam, V. Nayyeri, and O. M. Ramahi, "Microstrip Coupled-Line Directional Coupler for High-Sensitivity Dielectric Constant Measurement," in *2021 51st European Microwave Conference (EuMC)*, Apr. 2022, pp. 413–416.
[61] Z. R. Omam, V. Nayyeri, S.-H. Javid-Hosseini, and O. M. Ramahi, "Simple and High-Sensitivity Dielectric Constant Measurement Using a High-Directivity Microstrip Coupled-Line Directional Coupler," *IEEE Trans. Microw. Theory Tech.*, pp. 1–10, 2022.
[62] D. M. Pozar, *Microwave Engineering*, 4th ed. Hoboken, NJ: Wiley, 2012.
[63] G. Zysman and A. Johnson, "Coupled Transmission Line Networks in an Inhomogeneous Dielectric Medium," *IEEE Trans. Microw. Theory Tech.*, vol. 17, no. 10, pp. 753–759, Oct. 1969.
[64] S. Kiani, P. Rezaei, M. Navaei, and M. S. Abrishamian, "Microwave Sensor for Detection of Solid Material Permittivity in Single/Multilayer Samples With High Quality Factor," *IEEE Sensors J.*, vol. 18, no. 24, pp. 9971–9977, Dec. 2018.
[65] H. Lobato-Morales, A. Corona-Chávez, D. V. B. Murthy, and J. L. Olvera-Cervantes, "Complex permittivity measurements using cavity perturbation technique with substrate integrated waveguide cavities," *Rev. Sci. Instrum.*, vol. 81, no. 6, p. 064704, Jun. 2010.
[66] G. Federico, A. Reniers, A. Roc'h, L. Bronckers, and H. Visser, "Complex permittivity measurements with a low cost parabolic resonant cavity," in *The Loughborough Antennas Propagation Conference (LAPC 2018)*, Nov. 2018, pp. 1–6.
[67] Q. R. Marksteiner, M. B. Treiman, C.-F. Chen, W. B. Haynes, M. T. Reiten, D. Dalmas, and E. Pulliam, "Cavity resonator for dielectric measurements of high-ε, low loss materials, demonstrated with barium strontium zirconium titanate ceramics," *Rev. Sci. Instrum.*, vol. 88, no. 6, p. 064704, Jun. 2017.
[68] Keysight Technologies, "85072A 10-GHz Split Cylinder Resonator," *Technical Overview*.

Pau Casacuberta (GS'22) was born in Sabadell (Barcelona), Spain, in 1997. He received the Bachelor's Degree in Electronic Telecommunications Engineering and Computer Engineering from the Universitat Autònoma de Barcelona (UAB) in 2020, and the master's degree in Telecommunications Engineering in 2022. He received the Collaboration fellowship by the Spanish Government in 2019 for developing his Bachelor's Thesis in highly sensitive microwave sensors based in stepped impedance structures. Furthermore, he is currently working in the elaboration of his PhD, which is focused on the development of microwave sensors for the characterization of the composition of multicomponent liquid substances, with a research grant from FPU Program of the Universities Spanish Ministry.

Paris Vélez (S'10–M'14–SM'21) was born in Barcelona, Spain, in 1982. He received the degree in Telecommunications Engineering, specializing in electronics, the Electronics Engineering degree, and the Ph.D. degree in Electrical Engineering from the Universitat Autònoma de Barcelona, Spain, in 2008, 2010, and 2014, respectively. His Ph.D. thesis concerned common mode suppression differential microwave circuits based on metamaterial concepts and semi-lumped resonators. During the Ph.D., he was awarded with a pre-doctoral teaching and research fellowship by the Spanish Government from 2011 to 2014. From 2015-2017, he was involved in the subjects related to metamaterials sensors for fluidics detection and characterization at LAAS-CNRS through a TECNIOSpring fellowship cofounded by the Marie Curie program. From 2018 to 2020 he has worked in miniaturization of passive circuits RF/microwave and sensors-based metamaterials through Juan de la Cierva fellowship. His current research interests include the miniaturization of passive circuits RF/microwave and sensors-based metamaterials. Dr. Vélez is a Reviewer for the IEEE Transactions on Microwave Theory and Techniques and for other journals.

Jonathan Muñoz-Enano (S'19) was born in Mollet del Vallès (Barcelona), Spain, in 1994. He received the Bachelor's Degree in Electronic Telecommunications Engineering in 2016 and the Master's Degree in Telecommunications Engineering in 2018, both at the Autonomous University of Barcelona (UAB). Actually, he is working in the same university in the elaboration of his PhD, which is focused on the development of microwave sensors based on metamaterials concepts for the dielectric characterization of materials and biosensors.

Lijuan Su was born in Qianjiang (Hubei), China in 1983. She received the B.S. degree in communication engineering and the M.S. degree in circuits and systems both from Wuhan University of Technology, Wuhan, China, in 2005 and 2013 respectively, and the Ph.D. degree in electronic engineering from Universitat Autònoma de Barcelona, Barcelona, Spain, in 2017. From Nov. 2017 to Dec. 2019, she worked as a postdoc researcher in Flexible Electronics Research Center, Huazhong University of Science and Technology, Wuhan, China. She is currently a postdoc researcher in CIMITEC, Universitat Autònoma de Barcelona, Spain. Her current research interests focus on the development of novel microwave sensors with improved performance for biosensors, dielectric characterization of solids and liquids, defect detection, industrial processes, etc.

Ferran Martín (M'04-SM'08-F'12) was born in Barakaldo (Vizcaya), Spain in 1965. He received the B.S. Degree in Physics from the Universitat Autònoma de Barcelona (UAB) in 1988 and the PhD degree in 1992. From 1994 up to 2006 he was Associate Professor in Electronics at the Departament d'Enginyeria Electrònica (Universitat Autònoma de Barcelona), and since 2007 he is Full Professor of Electronics. In recent years, he has been involved in different research activities including modelling and simulation of electron devices for high frequency applications, millimeter wave and THz generation systems, and the application of electromagnetic bandgaps to microwave and millimeter wave circuits. He is now very active in the field of metamaterials and their application to the miniaturization and optimization of microwave circuits and antennas. Other topics of interest include microwave sensors and RFID systems, with special emphasis on the development of high data capacity chipless-RFID tags. He is the head of the Microwave Engineering, Metamaterials and Antennas Group (GEMMA Group) at UAB, and director of CIMITEC, a research Center on Metamaterials supported by TECNIO (Generalitat de Catalunya). He has organized several international events related to metamaterials and related topics, including Workshops at the IEEE International Microwave Symposium (years 2005 and 2007) and European Microwave Conference (2009, 2015 and 2017), and the Fifth International Congress on Advanced Electromagnetic Materials in Microwaves and Optics (Metamaterials 2011), where he acted as Chair of the Local Organizing Committee. He has acted as Guest Editor for six Special Issues on metamaterials and sensors in five International Journals. He has authored and co-authored over 650 technical conference, letter, journal papers and book chapters, he is co-author of the book on Metamaterials entitled *Metamaterials with Negative Parameters: Theory, Design and Microwave Applications* (John Wiley & Sons Inc.), author of the book *Artificial Transmission Lines for RF and Microwave Applications* (John Wiley & Sons Inc.), co-editor of the book *Balanced Microwave Filters* (Wiley/IEEE Press), co-author of the book *Time-Domain Signature Barcodes for Chipless-RFID and Sensing Applications* (Springer) and coauthor of the book *Planar Microwave Sensors* (Wiley/IEEE Press). Ferran Martín has generated 22 PhDs, has filed several patents on metamaterials and has headed several Development Contracts. Prof. Martín is a member of the IEEE Microwave Theory and Techniques Society (IEEE MTT-S). He is reviewer of the IEEE Transactions on Microwave Theory and Techniques and IEEE Microwave and Wireless Components Letters, among many other journals, and he serves as member of the Editorial Board of IET Microwaves, Antennas and Propagation, International Journal of RF and Microwave Computer-Aided Engineering, and Sensors. He is also a member of the Technical Committees of the European Microwave Conference (EuMC) and International Congress on Advanced Electromagnetic Materials in Microwaves and Optics (Metamaterials). Among his distinctions, Ferran Martín has received the 2006 Duran Farell Prize for Technological Research, he holds the Parc de Recerca UAB – Santander Technology Transfer Chair, and he has been the recipient of three ICREA ACADEMIA Awards (calls 2008, 2013 and 2018). He is Fellow of the IEEE and Fellow of the IET.